October 2022
Volume 1
Issue 1

Electrochemical Materials and Technologies

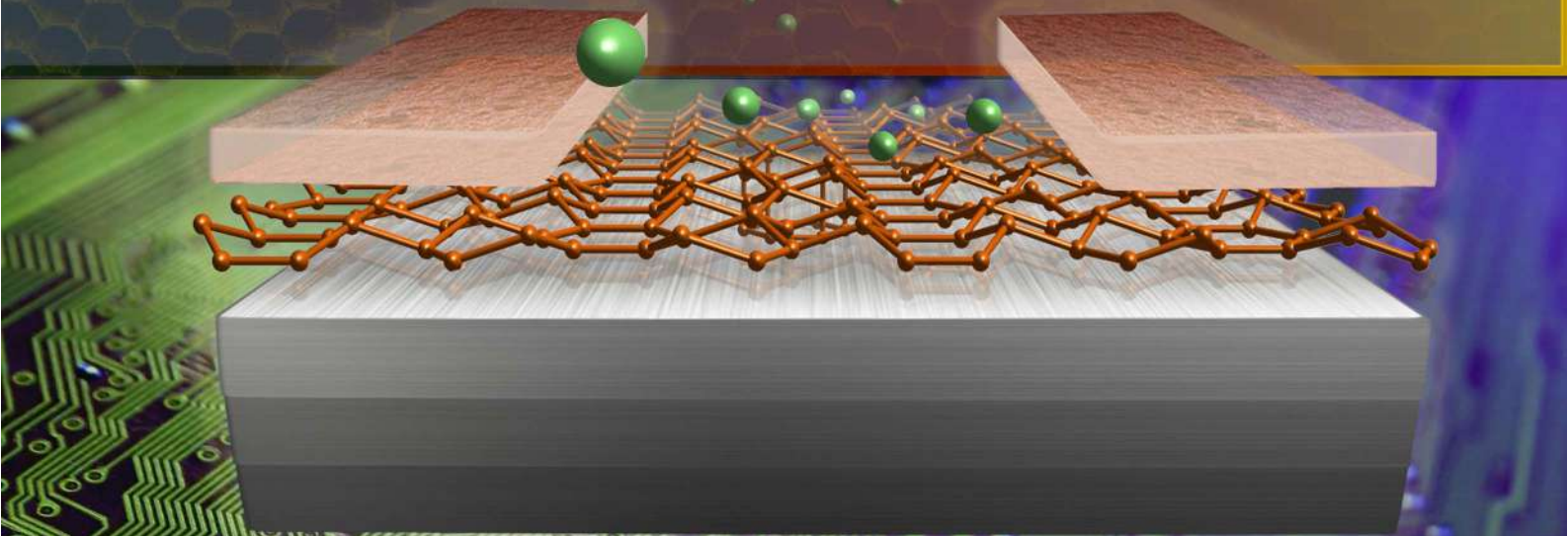

Ural Federal University
named after the first President of Russia B.N.Yeltsin

IHTE
Institute of High Temperature Electrochemistry
of Ural Branch of Russian Academy of Science

Electrochemical Materials and Technologies

REVIEW

Electrochemical Materials and Technologies

eISSN: 2949-0561

Cite this: Electrochem. Mater. Technol. 1 (2022) 20221005

Computer development of silicene anodes for lithium-ion batteries: A review

Alexander Galashev [ab *]

Received: 30 July 2022
Accepted: 30 September 2022

DOI: 10.15826/elmattech.2022.1.005

Lithium-ion batteries (LIB) have many advantages, the main ones being high energy density, long service life, small size, and low environmental pollution. This review is devoted to further development of LIBs based on quantum mechanical calculations in order to use them for energy storage in the future. Energetically favorite places occupied by lithium atoms on silicene are found. Lithium filling of free-standing two-layer silicene and single-layer silicene on graphene was studied. The geometric, energy, charging characteristics, as well as the open circuit voltage are determined. The effect of metallic (Al, Cu, Ni, Ag and Au) and non-metallic (C, SiC and BN) substrates on the geometric, energy and electronic properties of silicene has been studied. The effect of an intermediate nickel layer on the characteristics of the "silicene on a multilayer copper substrate" system has been studied. The effect of nuclear transmutation doping (NTD) of the silicene/graphite system with phosphorus on the density of electronic states of one- and two-layer silicene has been determined. Promising applications for silicene and the advantages of its use as an anode in a lithium-ion battery are discussed.

keywords: lithium-ion batteries, silicene, binding energy, DFT calculation, substrate

1. Introduction

1.1 Current and future lithium-ion batteries

Lithium-ion batteries have found widespread used for energy storage. The voltage of the battery is created by the movement of lithium ions. Lithium is the lightest metal and the most electropositive element used to create higher density energy storage devices. When a battery is charged, lithium ions move from the positive electrode to the negative electrode, passing through a separator. The separator in the form of a separating membrane avoids short circuits when the electrolyte supplies lithium ions. When the battery is powered by the load connected to it, the ions move in the opposite direction, and the electrons blocked by the separator pass through the load. Lithium batteries use unique active materials and chemical reactions to store energy. Currently, six of the most common lithium-ion batteries are in active use. Among them are Lithium Cobalt Oxide ($LiCoO_2$) batteries, which have the abbreviation LCO. Lithium Manganese Oxide ($LiMn_2O_4$) LMO, - Lithium Nickel Manganese Cobalt Oxide ($LiNiMnCoO_2$) - NMC, Lithium Iron Phosphate ($LiFePO_4$) - LFP, Lithium Nickel Cobalt Aluminum Oxide ($LiNiCoAlO_2$) - NCA, Lithium Titanate (Li_2TiO_3) - LTO batteries are also used often. Typical specific energies of these batteries are shown in Figure 1. It can be noted that NCA has the highest specific energy, but the specific power and thermal stability of LMO and LFP are higher than those of NCA.

a: Institute of High-Temperature Electrochemistry, Ural Branch of Russian Academy of Sciences, Yekaterinburg 620990, Russia
b: Ural Federal University named after the first President of Russia B.N. Yeltsin, Yekaterinburg 620002, Russia

* Corresponding author: alexander-galashev@yandex.ru

At the same time, LTOs have a longer life span. It has been established that the specific energy of a battery is determined by the specific capacities of the cathode and anode materials [1]. To achieve higher energy and power densities of LIBs, all new composites of active materials are used in the design of their elements. Thus, both separators and electrolytes are replaced. Their continuous improvement is carried out taking into account the increase in the safety of elements [2, 3].

Lithium-ion batteries are widely used in various fields. They are used as batteries for electric vehicles, smartphones, and other rechargeable systems. The anode material for LIB is currently graphite. The Li^+ concentrations up to which the adsorption/desorption processes can be performed are limited by the ratio C:Li = 6:1. As a result, the carbon anode limits the capacity of the battery and slows down the charging process. Thus, in order to create a new generation LIB, it is necessary to increase the capacity and charge/discharge rate in the battery operating cycle without increasing heat losses.

The most used anode materials at present are those based on graphite or based on metals alloyed with lithium. Anodes of the second type are safer in terms of dendritic formation and ignition. In addition, carbon anode batteries have low energy density and power. The disadvantage of a negative electrode made of a lithium-containing metal alloy is its low electrical conductivity and poor diffusion coefficient of Li+ ions. Among all anode materials studied, silicon proved to be the most suitable due to its highest theoretical specific capacity (about 4200 mAh g^{-1}), which is ten times higher than that of conventional carbon anodes (372 mAh g^{-1}) [4]. However, the practical application of silicon anodes is currently facing many problems.

The huge volume change (about 300%) at full lithiation creates an expansion/shrinkage stress during cycling. Ultimately, this leads to severe cracking of silicon and the formation of an unstable solid electrolyte interfacial phase (SEI) on the Si surface. The formed SEI contributes to the capture of lithium by the active material Si. The result is an irreversible rapid loss of capacitance at a low initial Coulomb efficiency (CE). The use of a silicon anode is also complicated by the very slow diffusion of lithium in Si (diffusion coefficient D = 10^{-14} – 10^{-13} cm^2 s^{-1}) and low intrinsic electrical conductivity of Si (10^{-5}–10^{-3} S cm^{-1}) [5–7].

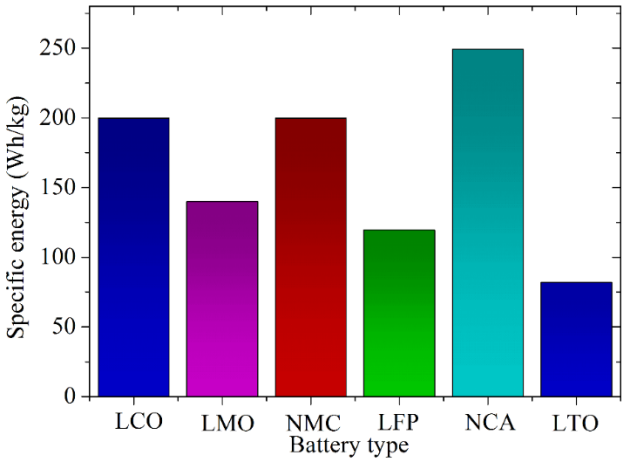

Figure 1 Typical specific energy of batteries.

Massive silicon anodes do not retain capacity well due to the large volume change during cycling. Film silicon nitride and silicon oxide anodes can serve as the alternatives [8–17]. They provide significant capacitance and good potential retention. The silicon anode was strengthened using a carbon additive, when C was introduced in the form of a Si–C composite or as a sealing layer on the Si surface [18–20]. However, a strong bonding tendency between Si and C results in the formation of silicon carbide (SiC) [18, 19]. For a time, SiC was thought to be an inactive anode material for LIB. However, subsequent studies have shown that SiC can be used as LIB anode. For example, when using it, a reversible capacity of 1200 mAh g^{-1} was achieved after 200 cycles [21]. It was shown that the reaction of transformation of SiC into elemental Si proceeds reversibly, followed by a reversible reaction of fusion/dealloying of Si with Li^+ [22].

Appropriately nanostructured materials have been used to improve the structural and electrical properties of silicon-containing anodes. Among them are nanotubes, nanowires, nanorods, as well as porous and hollow or encapsulating Si particles with protective coatings [23]. However, the production of such nanostructured materials is associated with a great complexity of technologies and multistage nature [24, 25], which makes the production of such anodes inefficient.

The rate of volumetric expansion of graphite during lithiation-delithiation is only about 10.6% [26]. Therefore, the use of silicon-carbon composite anodes seemed quite encouraging. Such anodes, as a rule, had higher capacitance and better cyclic stability [27]. However, poor first discharge efficiency and poor conductivity and cycling performance remain limiting factors for their application.

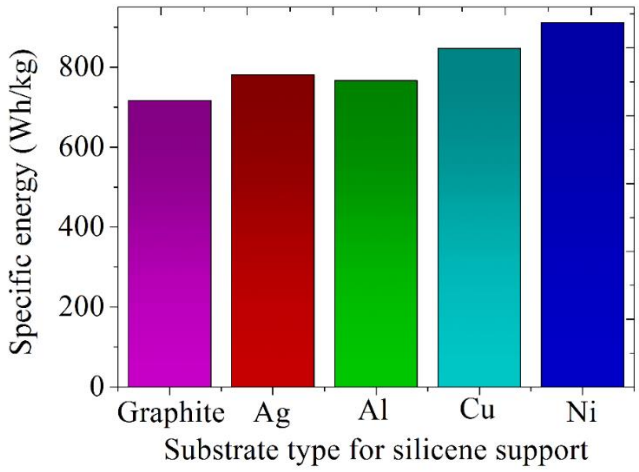

Figure 2 Estimated specific energies of batteries with a silicene anode placed on various types of substrates.

Recently, silicene has been intensively studied as an anode material for LIB [28–33]. Silicene differs significantly from graphene in a number of properties, including electronic properties and structure. At the same time, silicene has better mechanical properties that determine the material strength (Young's modulus and bulk modulus) than bulk crystalline silicon [34]. In addition, the adhesion of an atomic-thick silicon film to metal is much stronger than the adhesion between silicene and graphite. Silicene can be used as a complementary material to graphene if good technological control over such material exists [35].

The specific energies of batteries are mainly determined by the capacity of the anodes they use. The technique for assessing the anode capacitance includes determining the mechanical stability of silicene adsorbed by lithium [36–38]. Estimated specific energies of batteries with silicene anodes on metal (Ag, Al, Cu, Ni) and graphite substrates, obtained on the basis of the data on the mechanical strength of two-layer silicene [38], are presented in Figure 2. During the evaluation we considered a four-layer substrate material consisting of close-packed planes, as well as the energy of Si-Si bonds of silicene located on these substrates.

As can be seen from Figure 2, in the presence of a silicene anode with a Ni substrate in the battery, the specific energy of the battery is 27% higher than that of the battery having a silicene anode on a graphite substrate. The silicene-nickel anode is also the most effective among the silicene anodes formed on the metal (Ag, Al, Cu) substrates. A comparison of the data presented in Figures 1 and 2 indicates that the use of silicene anodes can increase the specific energy of batteries by 4.8 times on average.

1.2 Some ways of modifying anode materials

Battery life can be increased by various methods of physical or chemical attack on the anode material. For example, a carbon electrode can be irradiated with an electron beam to create strong C=C double bonds in the material. By chemically modifying the surface of the graphite anode, battery life can be greatly extended. The use of additives to the electrolyte makes it possible to suppress the destruction of graphite by the solvent. This also contributes to the charge transfer of Li^+ ions. Here we will look at a some more approaches to improve the quality of the 2D material, both for use in the LIB and for other applications.

Unmodified graphene is difficult to use in electronics because it is a zero bandgap semiconductor. Violation of the arrangement of atoms in the plane makes it possible to open the band gap. The electronic structure of graphene can be changed, for example, by mechanical deformation. Silicon belongs to the same group as carbon and has four valence electrons. The increase in the size of the silicon atom relative to the carbon atom is the main cause of warping of silicene. A large distance between Si atoms favors sp^3 hybridization. Low-buckled free-standing silicene is characterized by the σ–π orbital mixing, which is closer to sp^2 than to sp^3 hybridization. Graphene is the stiffest 2D material. The rigidity of warped silicene is about five times less than that of graphene. Low hardness values make it easy to introduce impurities. The introduction of larger atoms maintaining a covalent bond into a two-dimensional network leads to bond stretching and a decrease in the bond energy. The predominance of covalent and ionic interactions determines the bond strengths in the plane. However, long-range forces due to ionic interaction are not favorable for binding 2D structures.

Doping of semiconductors is usually carried out to change their electrical and optical properties. Impurities are divided into donors and acceptors. The former (donors) donate electrons to the conduction band, and the latter (acceptors) accept electrons from the valence band. Donors create n-doped materials, while acceptors create p-doped materials. Silicene has a strong corrugation which makes it difficult for ions to move between its sheets when using silicene as the anode material. The charging rate of LIB can be increased by

increasing the electrical conductivity of the anode. Heavy doping of silicene with phosphorus (group V element) adds additional uncompensated electrons to the system. The introduction of a donor in the form of phosphorus increases the electrical conductivity of the system. In addition, when doping silicene with phosphorus and graphene with nitrogen, the systems that include them can increase their strength. This is due to the fact that the strength of Si-P and C-N bonds is higher than the strength of Si-Si and C-C bonds, respectively [39, 40]. Nuclear transmutation doping allows one session of thermal neutron irradiation to transfer part of Si atoms into P atoms and part of C atoms into N atoms.

Silicene together with the substrate is a multilayer assembly designed for use in various devices. Assemblies with hybrid/hierarchical structures can include 2D materials with new custom properties. In this case, interlayer bonds can strongly affect both the possibility of interlayer separation and the electronic properties of the resulting heterostructures. Understanding the nature of the appearance of such bonds is important for the development of functional materials with desired characteristics. Ab initio calculations are the tool by which the initial structure, as well as the chemical and physical properties of 2D materials are calculated [41, 42]. In addition, these calculations help to find possible synthesis routes and understand the process of monolayer growth [42, 43].

The aim of the work is to test a new two-dimensional material - silicene for its suitability as an anode of a lithium-ion battery and to study in detail the conditions for its use, including the study of the effect of substrates on the stability of silicene and on its adsorption characteristics.

The review is presented from the standpoint of formation heterogeneous anode material including silicene: an introduction to the problem is provided in part 1, basic information about graphene and silicene is presented in part 2, the DFT calculation method and calculation of energy characteristics are described in part 3, polyatomic adsorption of lithium on a two-layer silicene and a single-layer silicene placed on graphene, is reflected in part 4, part 5 is devoted to the study of the effect of various substrates on the silicene anode, and finally, we briefly discuss the benefits of using a silicene anode in part 6.

2. 2D materials for energy applications

2.1 The first among open two-dimensional materials

In 2004, the first two-dimensional carbon material was obtained - graphene, which has a honeycomb structure and a thickness of one atom [44]. Graphene is represented as a single layer of graphite having a hexagonal lattice. The unit cell contains 2 carbon atoms. Due to sp^2 hybridization, C atoms in graphene are connected by strong sig and pi bonds. The tight binding method is well suited for describing the electronic structure of graphene [45, 46].

The band structure of graphene is distinguished by the presence of the Dirac cone, which suggests the existence of massless fermions, ultrahigh carrier mobility [47], and many other unusual properties [45, 48]. In particular, the possibility of achieving a half-integer [49, 50], fractional [51, 52], fractal [53–55] quantum Hall effect was discovered.

In suspended graphene, phase transitions between different fractional quantum Hall states were found [56]. The ultrahigh mobility of carriers in graphene, which is the most important consequence of the massless structure of the Dirac cone [48], has been experimentally verified. Graphene was studied on a Si/SiO_2 substrate, where charge impurities are the main source of scattering [57]. The mobility of carriers in graphene, limited by such scattering, was about 10^4 cm^2 V^{-1} s^{-1} at low temperature. Significantly higher mobility of carriers in graphene (~6×10^4 cm^2 V^{-1} s^{-1}) was achieved by placing graphene on an h-BN substrate [58]. This increase is due to the fact that the h-BN substrate is flatter and has fewer charge impurities. The theoretical mobility of carriers in graphene is 2×10^5 cm^2 V^{-1} s^{-1} at room temperature [59, 60]. Studies of suspended graphene showed that the mobility of carriers in graphene is limited by bending phonons at temperatures above 10 K [61]. It was also shown that both longitudinal acoustic (LA) and transverse acoustic (TA) phonons restrain the mobility of carriers in graphene [62].

Ripples ~1 nm high and ~10 nm in size were found in suspended graphene due to thermal fluctuations [63, 64]. Undoubtedly, such morphological changes affect the electronic properties of graphene. In particular, as a result of the action of ripples, nonzero densities of states at the Fermi energy and charge inhomogeneity (electron-hole pools) can form [65]. Corrugations can form on

graphene due to the roughness of the substrate. On SiO_2, the height of the corrugations can be 0.2 nm, and on mica, 0.02 nm [66]. Due to the presence of impurities, the substrate can induce an inhomogeneous charge distribution in graphene [67, 68]. The presence of a substrate can also lead to deformation, charge transfer, orbital hybridization, etc. The band gap of graphene can be opened using a large (up to 24%) uniaxial deformation [69]. Dirac cones are preserved under moderate uniaxial deformations. However, they are distorted and disappear when shear deformation is added [70]. Graphene deformation can be controlled by creating patterns on the substrate [71].

The discovery of graphene stimulated the search for other two-dimensional materials. Among a large number (more than 100) of discovering two-dimensional materials, there are compounds of group IV, binary systems of elements of groups III-V, metal chalcogenides, complex oxides, etc. [72, 73]. However, only some of them have a Dirac cone (graphene, silicene, germanene, several graphynes – sp-sp^2 carbon allotropes, and some others) [74–80]. Only Dirac cones in graphene received experimental confirmation [49, 50]. Graphene is a zero bandgap semiconductor. Therefore, unmodified graphene is difficult to use in electronics. Violation of the arrangement of atoms in the plane makes it possible to open the band gap. The electronic structure of graphene can be changed, for example, by mechanical deformation.

Graphene has extraordinary intrinsic strength. Young's modulus and Poisson's ratio of graphene are estimated as 1140 GPa and 0.19, respectively [81]. Graphene is used as fillers to obtain polymeric materials with better electronic conductivity. In epoxy polymer, an electric field is used to align graphene. Conductive polymer composites have conductivity in the direction of graphene alignment by 2–3 orders of magnitude higher than conductivity both along the transverse direction [82].

The lithium ions and electrons entering the graphite anode do not greatly distort its shape. Due to the slight deformation of the shape, the graphite anode is not subject to severe destruction during cycling, but has a capacity that does not meet the growing social demands. Graphene, as a single sheet of graphite, inherits its electrochemical properties. Therefore, its use in its pure form as an anode material is not advisable. However, the excellent strength properties of graphene and high electronic conductivity in plane make it a popular component for creating composite materials and heterogeneous structures. Recently, one-, two-, and three-dimensional carbon-based materials, as well as porous and core-shell structures, have been especially frequently studied for use as anode materials [83].

2.2 Obtaining silicene and its structure

The experimental synthesis of silicene on an Ag(111) substrate was carried out in 2012 [84]. It is from this moment that the modern era of silicene is counted. In fact, the atomic and electronic structure of silicene and germanene was established somewhat earlier. In 1994, Takeda and Shiraishi, using density functional theory (DFT), showed that the atomic structure of silicene and germanene is not perfectly flat, but contains buckles. The presence of buckles makes the structure of these two-dimensional materials energetically favorable. The band structure of these systems was also calculated, but no attention was paid to the presence of the Dirac cone in it. This article did not have the desired effect for two main reasons. First, doubts about the result obtained were dictated by the theoretical works of Peierls (1934) [85] and Landau (1937) [86], where it was shown that two-dimensional (2D) materials cannot exist in nature. Second, it seemed implausible that silicon could acquire sp^2-like hybridization, since it usually had sp^3 hybridization (Fagan et al. 2000) [87].

Silicon has a high tendency to oxidize. Therefore, the production of silicene must be carried out in an ultrahigh vacuum. In addition, the coating must be carried out under tight control to achieve sub-monolayer accuracy. Molecular beam epitaxy is currently the most preferred approach for fabricating silicon sheets. High demands are also placed on the purity of the substrate for the deposition of silicene. Most often, preference is given to a silver substrate obtained by repeated sputtering of argon ions and annealing. A silicon rod can be used as a source of Si. A stable flow of silicon is achieved by passing a constant electric current through it. The stability of the Si flow is due to a sufficiently high vapor pressure below the melting point of silicene. The substrate can be made not only from an Ag(111) single crystal, but also from an Ag film. This reduces the cost of the method for obtaining silicene devices.

The temperature and speed conditions of Si deposition on the substrate are of great importance for the production of silicene. If the substrate temperature is less than 400 K, the silicon atoms on the Ag(111) substrate tend to form clusters or disordered structures [88]. When the substrate temperature exceeds 400 K, 5 more often than other observed and even more different ordered phases can be formed [89–92]. Such a variety of forms of reconstruction is associated with the multiplicity of possibilities for warping silicene. At present, there is no consensus on the various phases of silicene grown on Ag(111) [93].

The silicene phases obtained as a result of reconstruction are designated in the literature, both by the Si lattice type and by the Ag lattice type. To avoid confusion, it makes sense to define both phases. For example, if the silicene phase is defined as 3×3 and the Ag phase is defined as 4×4, then it is possible to designate this silicene phase on the Ag substrate as Si(3×3)/Ag(4×4). One of the first to be discovered was the so-called T-phase [88], whose structural model was built on the following experimental facts:

(i) This phase appears at the lowest temperature regime, at which ordered phases of silicene already appear. Other phases do not occur in this mode.

(ii) This phase has a periodicity different from other ordered phases. In addition to the hexagonal close packing indicated by large protrusions, there are parallel linear chains formed by structural units.

(iii) This phase turns out to be a partially disordered phase formed from local silicene fractions with incomplete ordered packing. It can be considered as a "predecessor phase" for more ordered phases such as 4×4 and $\sqrt{13} \times \sqrt{13}$.

The T phase can be considered as a “precursor” for the formation of the 4×4 phase [88]. However, the island structure of silicene without hydrogen bonding is unstable [94]. For better joining, the hexagonal rings can be deformed by allowing a new warping of the silicene. As a result, the T-phase obtained by this method has a flatter structure compared to free-standing silicene.

The ideally ordered phase, designated 3×3 with respect to silicene and 4×4 with respect to the Ag(111) substrate, is the first hexagonal phase that appears at a relatively low substrate temperature. Such a structure is formed due to the excellent correspondence between the four lattice constants of Ag(111) (a_{Ag} = 2.88 Å) and the three lattice constants of Si (a_{Si} = 3.84 Å), the mismatch is no more than 0.5%. In other words, the Si(3×3)/Ag(4×4) superstructure is easily constructed by superimposing a free-standing low-bending silicene 1×1 lattice on an Ag(111) –1×1 lattice in the same orientation. In this case, the deformation of the interface turns out to be minimal, which stabilizes the silicene structure. At the domain boundaries between the α-4×4 phases, one can also observe the 4×4-β phase, which has the same periodicity as the α-4×4 phase [95]. The border 4×4-β phase is less stable than the main α-4×4 phase. Its stabilization is facilitated by the deformation of the domain boundary.

The $\sqrt{13} \times \sqrt{13}$R13.9° ($\sqrt{13} \times \sqrt{13}$ for short) phase as a rule, is always observed together with the 4×4 phase [96–100]. The silicene film formed by these phases can completely cover the surface of the substrate. By changing the annealing temperature, one can change the ratio of areas covered by each of these phases. However, it is practically impossible to obtain a single-phase surface, since both phases have comparable thermal stability. In addition, the densities of these phases are approximately the same, so that the total area of the silicene film does not change with the annealing temperature.

3. Calculation method. Energy estimations

3.1 Method of calculation

Due to the fact that the methods for obtaining silicene are currently not sufficiently perfect, it is not yet possible to carefully study the functioning of silicene anodes experimentally. We restrict this review to consideration of computational works devoted to the study of silicene anodes. Moreover, we mainly pay attention to works performed on the basis of first-principles calculations, including those using ab initio molecular dynamics (MD).

Since the possibility of obtaining stable free-standing 2D crystals is called into question due to the works of Peierls [85] and Landau [86], the question of studying the stability of 2D crystals comes to the fore. The instability of ideal two-dimensional crystals appears due to the suppression of long-wavelength phonons, which causes lattice melting at $T > 0$.

The static stability of single-element 2D materials can be established by calculating stiffness tensors, Young's modulus, and Poisson's ratios [101]. The dynamic stability is determined

from the calculated phonon dispersion of these materials. The imaginary modes on the dispersion curves of phonons indicate the dynamic instability of the structure. An abnormal decrease in the characteristic frequency resulting in mechanical instability is defined as a "soft mode". The dynamic instability created by the "soft mode" can be fixed in a cell that has the shape of a hexagonal ring [102] (Figure 3). Figure 3 also shows a figure (rhombus) that determines the directions for laying hexagonal cells (honeycombs), as well as the characteristic directions (armchair and zig-zag) of anisotropy in the resulting packing.

When using silicene devices whose operation leads to the creation of dynamic loads in a two-dimensional material, attention should be paid to the mechanical properties of silicene. Morphologically, silicene differs from graphene in that graphene is completely flat, while silicene exhibits a significant level of buckling. This happens because of the rather strong bond between unoccupied molecular orbitals and occupied molecular orbitals in silicene. This so-called Jan Teller pseudo-effect [103] introduces instability in highly symmetrical configurations. As a result, the atoms in silicene are not in purely sp^2 hybridized states. The wrinkling of silicene leads to a decrease in the rigidity of the plane and provokes the formation of linear chains of atoms. The values of Young's moduli for silicene are practically isotropic, while the critical strain is not isotropic [104]. Under similar conditions, graphene is many times (~10 times) stronger than silicene.

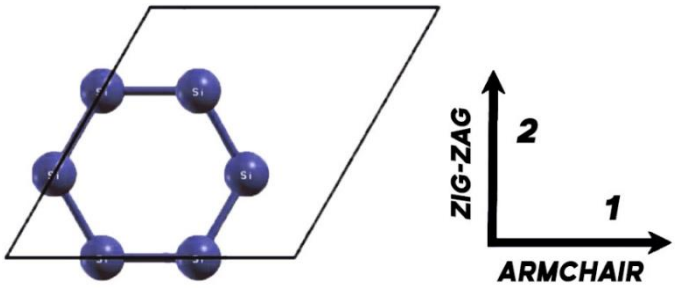

Figure 3 The conventional silicene hexagonal cell (ring of 6 atoms) in the undeformed reference configuration.

DFT calculations make it possible to determine the forces on each atom, the total energies of the system, stresses, and stress–strain relationships of silicene under the desired deformations. The SIESTA modeling package used for the calculation is based on the Kohn–Sham Density Functional Theory (KS-DFT) [105]. Exchange-correlation functions are represented using the generalized gradient approximation parameterized by Perdew, Burke, and Ernzerhof (PBE) [106]. The $3s^23p^2$ electrons in silicon atoms are explicitly included in the calculation. The core electrons are modeled using the projector augmented wave (PAW) and pseudo-potential approach [107]. A plane-wave cutoff was performed at a level of 400 Ry in many calculations [29, 36–38, 93]. MD ab initio calculations were performed at a temperature of 300 K.

The original geometric structures were initially optimized. The relaxation of the electronic degrees of freedom stopped when the change in the total energy was less than 0.00001 eV. Also, all initial atomic structures were subjected to geometric optimization. Moreover, the criterion for the minimum forces acting on each atom was the value of 0.001 eV $Å^{-1}$. The expansion of the system was performed by the periodic (Born-von Karman) boundary conditions, with the help of which a physical quantity was translated into a Fourier series, using the set of all plane waves that satisfy the boundary condition.

The numerical errors caused by the deformation of the system were leveled out by using a sufficiently large 10× 10×1 k-grid representing the Brillouin zone. The Brillouin zone of undeformed silicene with high symmetry points is shown in Figure 4. In a number of papers discussed here, the band structures in direction -M-K- of the systems were calculated, where points Γ, M, and K are points of high symmetry in reciprocal space.

A vacuum region 15 Å thick separated the system from its image in the vertical direction. At first-principles MD calculations, the Nose-Hoover thermostat [108] was used, with the help of which the temperature was maintained at 293 K. The time step length was 1fs, and the duration of each calculation was 2000 time steps.

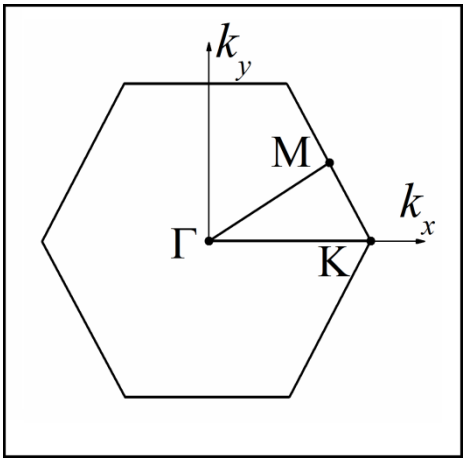

Figure 4 Brillouin zone with points of high symmetry.

3.2 Energy estimates of lithiated silicene

Study of the nature of the interaction between lithium and silicene occupies one of the central places in testing silicene for the suitability of its use in electrochemical devices. The energy and stability of partially and fully lithiated silicene was studied using MD modeling based on density functional theory (DFT) in [109]. Overall, this study showed that lithiated silicene is more stable, relative to its bulk counterpart, than bare silicene.

The strength of the Li-Si bond in the Li_xSi_{1-x} compound was estimated from the adsorption energy of lithium atoms on both sides of the silicene surface. The adsorption energy, or binding energy, was determined according to the expression:

$$E_{ad} = \frac{E_{Si} - N_{Li}E^1_{Li} - E_{Si+Li}}{N_{Li}}, \quad (1)$$

where E_{Si}, E_{Si+Li}, and E^1_{Li} are energies calculated for free-standing silicene, the silicene/lithium subsystem and the lithium adatom, respectively, and N_{Li} is the number of lithium atoms in the system.

The adhesion energy between lithium and silicene was calculated according to the expression:

$$E_{adh} = \frac{E_{Si+Li} - N_{Li}E^1_{Li} - N_{Si}E^1_{Si}}{N_{Li}+N_{Si}}, \quad (2)$$

where N_{Si} is the number of Si atoms in the system, E^1_{Si} is the total energy of a single silicon atom.

The Gibbs free energy of formation reflects the stability with respect to the bulk analogs of Li and Si, and it is given by

$$\delta G = E_{adh}(x) - xU_{Li} - (1-x)U_{Si}, \quad (3)$$

where U_{Li} and U_{Si} are the chemical potentials of bulk lithium and silicon, respectively.

The U_{Li} values are 1.612 and 1.794 and U_{Si} are 5.426 and 6.123 eV/atom in the GGA and LGA cases, respectively. The chemical potential of bulk silicon is defined as −4.63 eV/atom [110].

In [108], four main possible sites for the adsorption of lithium atoms in an eight-atom silicene supercell were considered, including a hollow, a bridge, an atom up, and an atom down sites. The most energetically favorable is the configuration obtained by adsorption of eight lithium atoms, i.e. at lithium concentration x_{Li} = 0.5. This state is reached when all "atom down" locations are filled. A fully lithiated silicene sheet, when each Si atom is bonded to a Li atom, is commonly referred to as silicel. The calculated adsorption energy for silicel E_{ad} is 2.394 eV/Li. Figure 5 shows the optimized silicel configuration and bond length data.

Figure 6 shows the adsorption energy for all configurations with the lowest U_{ad} value. The calculated adsorption energies for partially and fully lithiated silicene range from 2.210 to 2.515 eV/Li, and the average Si-Li bond length is 0.2639 nm. These data indicate strong chemisorption of lithium on silicene in all cases considered. Although the adsorption energy reflects the strength of the Li–silicene interaction, it does not describe adequate connection stability. In particular, despite the fact that the adsorption energy at x_{Li} = 0.33 is maximum, this type of lithiation does not give the most stable structure corresponding to the minimum Gibbs free energy.

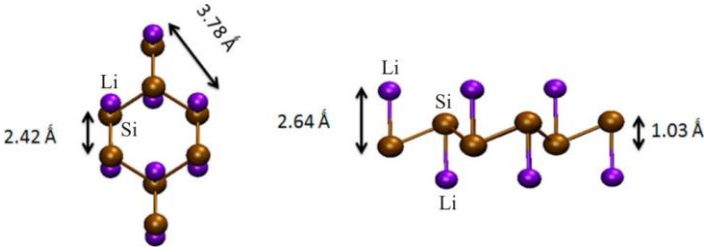

Figure 5 Relaxed geometric structure of fully lithiated silicene (silicel) obtained using GCA [108].

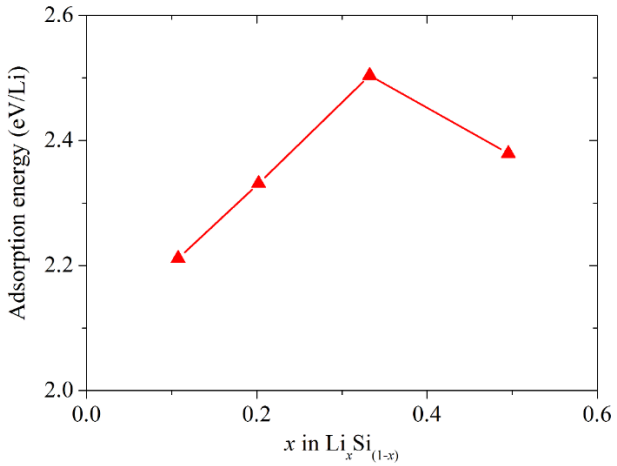

Figure 6 Dependence of lithium adsorption energy on lithium content on silicene for configurations with the lowest adsorption energies [108].

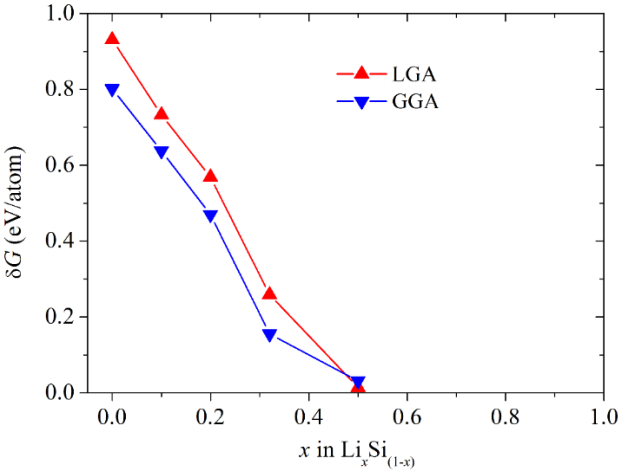

Figure 7 Changes in the Gibbs free energy of the LixSil-x compound with increasing lithium content, obtained using LGA and GGA. The cases of pure bulk Si and pure bulk Li are presented as δG = 0. For fully lithiated silicene, the difference between the LGA and GGA in Gibbs energy changes is 3 meV/atom [108].

To evaluate the stability of partially and fully lithiated silicene sheets, the Gibbs free energy change δG was calculated for each structure. These values are reflected in Figure 7. It should be noted that the difference between the results of GGA and LDA is small (the maximum difference for δG of pure silicene is 15%). This difference does not affect the stability trend and other findings. Shown in Figure 6, δG is the energy of formation for each compound. A positive δG value indicates that the formation is endothermic and produces a less stable structure. It can be seen that with an increase in the lithium content, the stability of the structure approaches the stability of a bulk compound with the same atomic ratio. The GGA (LDA) energy of formation of 0.015 (0.012) eV for $Li_{0.5}Si_{0.5}$ suggests that fully saturated silicene is essentially as stable as a bulk compound with the same lithium content.

4. Investigation of Li and Na filling of silicene and silicene/graphene anodes

4.1 Filling a flat silicene channel with lithium

The channel for filling with lithium was formed by two silicene sheets located one above the other, the gap between them was 0.75nm. The characteristics important for the analysis of the functioning of the silicene anode were calculated [22]. Among them are the cohesive energy, open-circuit voltage (OCV), the total Voronoi charge [111] transferred by lithium and the distance between the walls of the silicene channel.

The binding energy between lithium atoms without taking into account the effect of silicene was determined as

$$E_b^{\mathrm{Li}} = \frac{E_{\mathrm{Li}} - N_{\mathrm{Li}} E_{\mathrm{Li}}^1}{N_{\mathrm{Li}}}, \quad (4)$$

where E_{Li} is the total energy of the lithium subsystem excluding influence of the silicene sheets.

The bond energy between silicon atoms in the silicene sheet without taking into account the influence of lithium and the second silicene sheet is given by

$$E_b^{\mathrm{Si}} = \frac{E_{\mathrm{Si}}^{l/u} - N_{0.5\mathrm{Si}} E_{\mathrm{Si}}^1}{N_{0.5\mathrm{Si}}}, \quad (5)$$

where $E_{\mathrm{Si}}^{l/u}$ is the energy, calculated for the lower or upper silicene sheet and $N_{0.5\mathrm{Si}}$ is the number of silicon atoms in one silicene sheet.

The gravimetric capacity of the battery cell in question can be determined as:

$$C_{TS} = xF/M, \quad (6)$$

where x is the number of interacting electrons, F is the Faraday number, M is the molar mass of the system.

The open circuit voltage can be calculated according to:

$$\mathrm{OCV} = (E_{\mathrm{Si}} + N_{\mathrm{Li}} E_{\mathrm{Li}}^1 - E_{tot})/n_e, \quad (7)$$

where E_{tot} is the total energy of the entire system, n_e is the number of valence electrons in the system.

Table 1 – Dependence of the energy characteristics* of a free-standing silicene sheet adsorbed by lithium on the number of settled Li atoms [22].

N_{Li}/N_{Si}	E_b, eV	E^{Si}_b, eV	E^{Li}_b, eV	E_{adh}, eV	BG, eV
0.0625	-4.631	-4.786	-	2.154	M
0.125	-4.491	-4.745	-0.236	2.219	M
0.1875	-4.375	-4.685	-0.252	2.474	M
0.25	-4.273	-4.658	-0.511	2.223	0.411
0.3125	-4.161	-4.677	-0.548	1.961	M
0.375	-4.075	-4.649	-0.686	1.858	0.474
0.625	-3.782	-4.596	-0.908	1.574	0.134
0.875	-3.599	-4.557	-1.088	1.417	0.409
1	-3.541	-4.520	-1.172	1.390	0.645
1.125	-3.408	-4.551	-1.180	1.212	M
1.375	-3.250	-4.279	-1.275	1.227	M
1.625	-3.052	-4.518	-1.278	0.871	M
1.875	-2.942	-4.492	-1.343	0.772	M
2.125	-2.832	-4.520	-1.385	0.652	M
2.375	-2.755	-4.530	-1.407	0.601	M

* E_b is total binding energy of all atoms in the system; E^{Si}_b is binding energy of silicon atoms in a silicene sheet; E^{Li}_b is binding energy between lithium atoms in the lithium subsystem; E_a is adhesion energy between lithium and silicene sheet; BG is band gap.

The voltage profile was calculated according to the method proposed in [36, 112] as:

$$V(N) = \frac{(E^{N_2}_{\mathrm{LiSi}} - E^{N_1}_{\mathrm{LiSi}} - (N_2 - N_1)E^{m}_{\mathrm{Li}})}{(N_2 - N_1)n_e}, \quad (8)$$

where $E^{N_2}_{\mathrm{LiSi}}$ and $E^{N_1}_{\mathrm{LiSi}}$ are the total energies of systems containing N_2 and N_1 lithium atoms, and E^{m}_{Li} is the total energy calculated for metallic lithium.

The calculated energy characteristics presented by expressions (2), (4) and (5) together with the band gap created in silicene are presented in Table 1. As the number of lithium atoms in the system increases, the total binding energy and the bonding energy between silicon atoms decreases in absolute value. Although after N_{Li}/N_{Si} = 1 this decrease for the Si-Si bond becomes non-monotonic. There is an increase in the lithium atoms binding with an increase in Li density in the channel. At N_{Li}/N_{Si} = 0.25 and in the range 0.375 ≤ N_{Li}/N_{Si} ≤ 1, free-standing lithiated silicene becomes a narrow-gap semiconductor, while at other considered values of adsorbed lithium, it exhibits conducting properties.

The dependence of these characteristics on the ratio of lithium to the silicon atoms is shown in Figure 8. As can be seen from the figure, the adhesion energy passes through a minimum, which is observed at N_{Li}/N_{Si} = 1. At the ratio N_{Li}/N_{Si} = 1, the filling of the channel with lithium does not lead to the formation of defects in silicene. In this case, the gravimetric capacity of the system is 954.3 mAh/g. The maximum filling of the channel with lithium is achieved at N_{Li}/N_{Si} = 2.3, which corresponds to a gravimetric capacity of 2223.5 mAh/g. It can be seen from the Figure that OCV continuously increases with an increase in the N_{Li}/N_{Si} ratio. There is an empirically established limit to the OCV value. If its value exceeds 1 V, then dendrites can form in the system. For the system studied in [37], the OCV value is always less than 1. Extrapolation of the obtained dependence for OCV indicates that dendrites between the electrodes can form only at N_{Li}/N_{Si} = 3. The total Voronoi charge,

having reached a maximum at N_{Li}/N_{Si} = 1.25, decreases with a further increase in the considered argument. The distance between the walls of the silicene channel increases nonmonotonically as the N_{Li}/N_{Si} ratio increases. When the channel is initially filled with lithium until the value N_{Li}/N_{Si} = 0.4 is reached, the channel, which has an initial gap of 0.75nm, narrows. When the density of lithium in the channel is low, the channel walls are pulled towards each other through it. However, in the N_{Li}/N_{Si} range from 0.5 to 1.8, the distance between the channel walls again increases from 0.3079 to 0.7088nm. This increase occurs when density of filling the channel with lithium requires an expansion of the channel gap. When the N_{Li}/N_{Si} ratio changes from 2 to 2.3, the gap increases from 8.054 to 8.955 Å, i.e., it becomes even wider than it was at the beginning of the calculation.

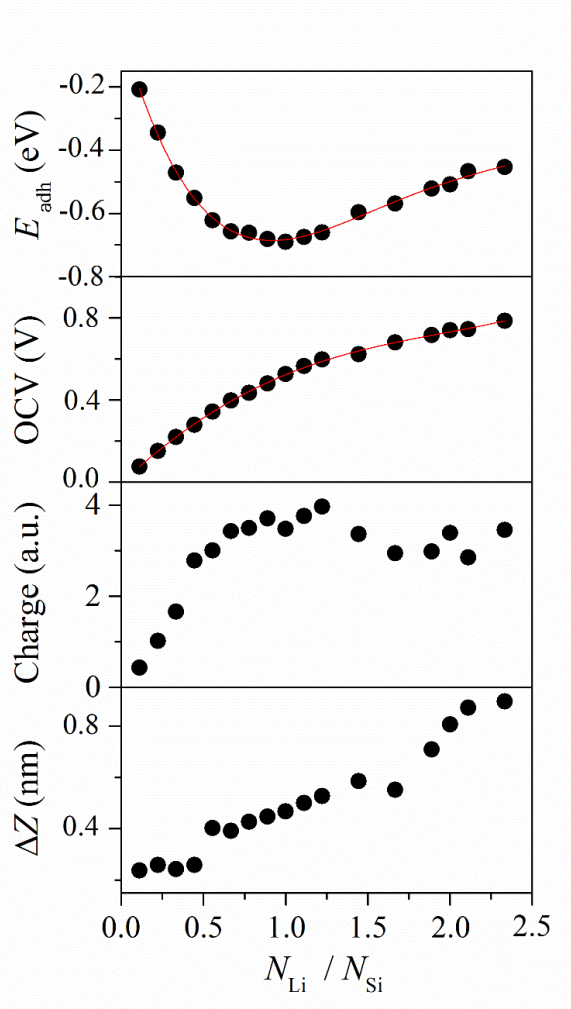

Figure 8 The adhesive energy between the silicene sheets and the lithium surface, open-circuit voltage, total Voronoi charge carried by lithium, and the gap between the walls of the silicene channel as a function of the ratio of lithium and silicon atoms in the system.

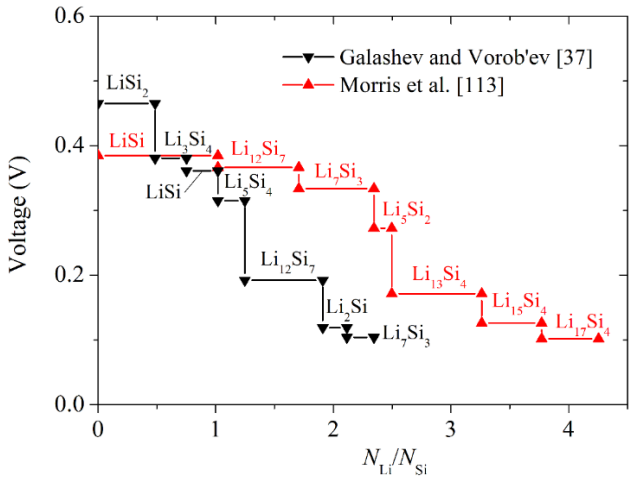

Figure 9 Voltage profile plotted depending on the ratio of lithium atoms to silicon atoms in the channel.

The movement of a charged particle between the electrodes causes a change in the potential. There is a stepwise decrease in the stress profile with increasing Li/Si ratio (Figure 9). The flat areas on the graph reflect the observed Si-Li phases. MD calculations show that the system goes through the following sequence: $LiSi_2$, Li_3Si_4, LiSi, Li_5Si_4, $Li_{12}Si_7$, Li_2Si, and Li_7Si_3. Figure 9 also shows the voltage-age profile obtained using the DFT method in conjunction with the random structure searching method [113]. It can be seen that ab initio MD calculations indicate a steeper descent of the voltage profile.

Most of the phases obtained in the MD calculation [37] were also found in [36], where it was shown that lithium interacts with silicene more strongly than graphene.

4.2 Ab initio simulation of silicene/graphene anode for Li and Na ion batteries

The currently used lithium-ion batteries, operating with a graphite anode cannot provide satisfactory performance [114–116]. There are new requirements for energy storage devices, which include large capacity, high charging speed, good cycle performance and low price. As an anode material, it is proposed to use two-dimensional (2D) materials, the unique properties of which are largely determined by their structure [117–123]. These materials have a large surface area to accommodate lithium atoms. In addition, the relatively large distance between the 2D layers should moderate the volumetric expansion and contraction caused by lithium intercalation and deintercalation. The advantages of using lithium in a rechargeable battery are the small size of this ion, the ease of diffusion with a low energy

barrier, and the large penetration depth. However, the meager distribution of lithium in the Earth's crust makes it an expensive material. The abundance of the sodium element determines its low price [124–126]. Sodium-ion batteries are still being considered as an alternative to lithium-ion batteries. However, the diffusion of sodium ions is not as easy as the diffusion of lithium ions. Due to their larger size and weight, sodium ions cannot penetrate as deeply into the material as lithium ions. However, when using two-dimensional materials with weak van der Waals interactions between layers to construct an anode, it is possible to create a sodium-ion battery. In this case, the main problem is to neutralize the large volume expansion caused by sodium intercalations in order to maintain structural integrity [127–131].

It is known that a strong interaction between a metal substrate and silicene leads to the disruption of the electronic structure of the initial silicene [132] and can also cause surface reconstruction [133]. However, to support silicene, graphene can be used instead of a metal substrate [134, 135]. The interaction between silicene and graphene is due to van der Waals forces, as a result of which the internal properties of silicene are largely preserved. Due to the high strength characteristics of graphene, the silicene/graphene heterostructure should have better mechanical properties. However, it is necessary to study the adsorption properties of such a heterostructure in order to estimate the capacity of the anode built on its basis. In addition, good structural stability of the silicene-graphene anode must be ensured during the charge/discharge process for both lithium and sodium.

The diffusion properties of lithium and sodium in the silicene/graphene heterostructure were studied. The energy barriers for the diffusion of lithium and sodium over the surface of silicene were 0.36 eV and 0.22 eV, respectively [29]. Additional tests of the behavior of Li and Na atoms on the graphene surface and in a channel formed on one side by a silicene sheet, and on the other side by a graphene sheet, showed that the energy barriers to diffusion are below 0.40 eV for lithium and less than 0.30 eV for sodium. Such energy barriers provide high charging rates when using silicene/graphene anode in metal (Li or Na) ion batteries.

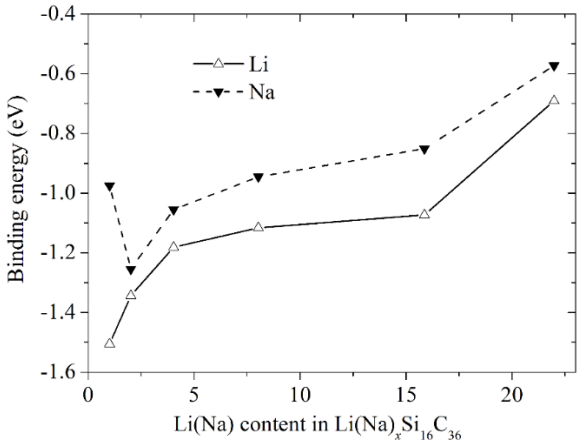

Figure 10 The binding energy of lithium and sodium adsorption onto the silicene/graphene heterostructure at different Li (Na) concentrations.

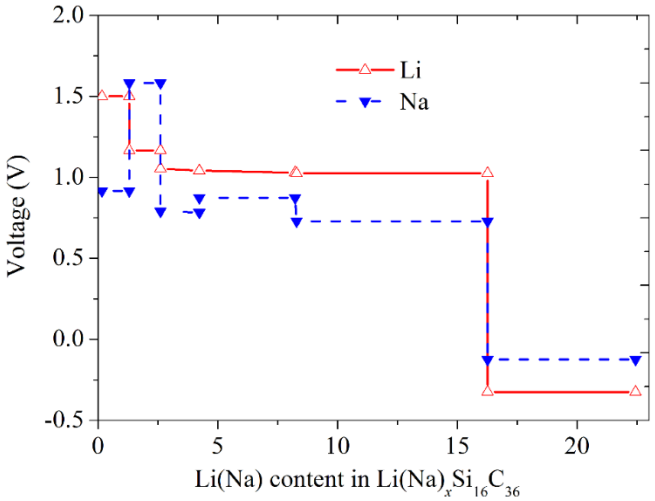

Figure 11 The calculated voltage profiles along with the lithiation/sodiation process.

The adsorption of Li and Na atoms on a silicene/graphene heterostructure was studied at ratios of the number of alkali metal atoms to the number of heterostructure atoms from 0.02 to 0.42. The binding energies of lithium and sodium at their various concentrations are shown in Figure 10. These energies are negative at all considered concentrations. It can be seen that strong adsorption is retained at high concentrations of Li and Na. Therefore, the use of a silicene/graphene heterostructure as an anode will allow it to store a large amount of charge carriers on this electrode.

The evaluation of the open circuit voltage was performed according to equation (7). This characteristic is shown in Figure 11. As can be seen from the figure, the OCV becomes negative when the concentration of Li or

Na reaches a value of 0.42. This concentration corresponds to a capacity of 487 mAh g^{-1} when Li or Na atoms are completely adsorbed on the outer surface of silicene and on the inner surfaces that form the space between silicene and graphene. The average OCV value for the considered heterostructure is 1.07 V. when used as charge carriers of lithium ions and equal to 0.84 V when used as carriers of sodium ions. Such OCV values do not allow for the formation of dendrites and provide a high energy density. Thus, the use of silicene/graphene heterostructure as an anode material makes it possible to create good performance characteristics of the battery and provides mechanical rigidity of the anode.

5. DFT study of the behavior of silicene on various substrates

In addition to the Ag(111) substrate [136], silicene was later obtained on a number of other substrates. It was epitaxially synthesized on Ir (111) [137], Au [138], Ru (0001) [139], MoS_2 [140], ZrB_2 (0001) [141], ZrC (111) [142], and graphite [143] substrates. The interactions of silicene with silver [30, 33, 144], copper [30, 144, 145], aluminum [30, 32, 144, 146], nickel [4, 30, 144, 147], nickel with copper impurity [148], graphite [149–151], nitrogen doped graphite [31, 34, 152–154], and silicon carbide [155] substrates were studied by classical MD methods. Al adsorption on silicene was studied using DFT calculations in [156]. Dense two-sided adsorption of Al on silicene led to an unstable configuration. The chemical separation method with $CaSi_2$ as a precursor was used to synthesize "autonomous" silicene [157].

5.1 Metal and carbon substrates

DFT modeling of silicene placed on metal (Al, Cu, Ni, Ag, and Au) substrates was performed in [158–160] and on a graphite substrate in [4]. The use of SIESTA [161] or VASP [162] programs without changing the basic codes when modeling heterostructures, extended by periodic boundary conditions, require the creation of a single period of spatial translations. In other words, it is necessary, by means of scaling, to match the superlattices for all the components that make up the system. Superlattice alignment required an increase in translation vectors by 4% in the aluminum and silver substrates and by 3% in the gold substrate. In the case of Si and Cu, the mismatch of supercells, which is ~2%, does not require additional operations for alignment. To combine the C-Si and Ni-Si systems, modified superlattices were taken: the silicene cell was increased by 4%, and the graphite (nickel) cell was reduced by 4%. The substrate thickness varied from 1 to 5 (4 layers in the case of a graphite substrate) layers. This was enough to determine the optimal number of layers (i.e., limiting their number) to perform accurate calculations for "silicene on metal film" systems. Approximate modeling of silicene on bulk metal (Al, Cu, Ni, Ag and Au) substrates can be performed similarly by adding an additional lower metal layer to the optimally obtained metal substrate, the atoms of which are fixed in the z direction.

Figure 12 shows the types of combined silicene-metal supercells. The silicene sheet was parallel to the xy plane. To simulate silicene on substrates, 2×2 (C, Cu, and Ni substrate) or 3×3 (Al, Ag, and Au substrate) supercells were used. The silicene structure is represented by two sublattices (lower and upper) spaced 0.44 Å apart. The substrate layers had 3×3 (C, Cu, Ni) or 4×4 (Al, Ag, Au) supercells.

Table 2 presents the calculated adhesion energies between silicene and the substrate obtained for various substrate thicknesses. The adhesion energy when adding layers varies in a very different way depending on the substrate material. For example, when going from one layer to two layers for Ag and Au substrates, E_{adh} almost doubles, which does not occur in the case of other types of substrates under consideration. It is noteworthy that in the end, E_{adh} ceases to change much when the next layer is added. This happens by adding a fifth layer for all metal substrates and a fourth layer to the carbon substrate.

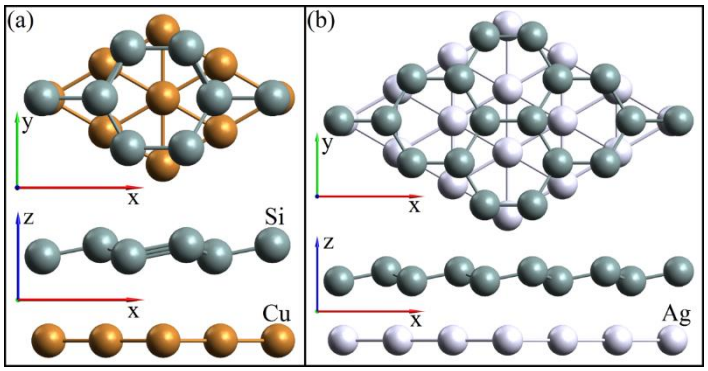

Figure 12 An example of superlattice alignment: (a) 2x2 silicene and 3x3 copper (111), (b) 3x3 silicene and 4x4 silver (111).

Table 2 – Adhesion energies (eV/cell) between silicene and substrates depending on the number of layers in the substrate.

N_{Sub}	C	Al	Cu	Ni	Ag	Au
1	0.284	1.626	1.719	3.599	0.698	0.696
2	0.300	1.424	1.857	3.432	1.249	1.028
3	0.309	1.284	2.007	2.945	1.229	1.024
4	0.306	1.137	1.999	2.881	1.256	1.054
5	-	1.144	1.997	2.899	1.241	1.046

Table 3 – Characteristics* of systems «silicene on substrates» with a fixed bottom layer after geometric optimization

Substrate	L_{Si-Si}	L_{Si-Sub}	$L_{Sub-Sub}$	Δ_{Si-Si}	Δ_{Si-Sub}	E_b^{Si}	E_{adh}
C	2.259	3.576	1.447	0.626	3.495	4.408	0.300
Al	2.379	2.745	2.906	0.821	2.362	5.274	1.136
Cu	2.377	2.577	2.639	1.127	2.045	5.608	2.014
Ni	2.307	2.404	2.524	0.897	1.848	6.234	2.873
Ag	2.371	2.859	2.936	0.831	3.070	5.318	1.263
Au	2.394	2.920	2.980	1.190	3.151	5.197	1.063

*Parameter designations are described in the text.

Some characteristics obtained in the model representing silicene on a "massive" metal or carbon substrate are presented in Table 3. The massiveness of the substrate was created by pinning the z-coordinates of the lower layer of the substrate. The characteristics placed in Table 3 are L_{Si-Si} is the average bond length between silicon atoms in a silicene sheet; L_{Si-Sub} is the average bond length between the silicon atoms of the silicene sheet and the atoms of the substrate; $L_{Sub-Sub}$ is the average bond length between substrate atoms; Δ_{Si-Si} is the distance between silicene sublattices; Δ_{Si-Sub} is the distance between the bottom sheet of silicene and the metal substrate; E_b^{Si} is the binding energy between silicon atoms in a silicene sheet; E_{adh} is the adhesion energy between the silicene sheet and the substrate.

From a comparison of the data in Tables 2 and 3, it can be seen that the adhesion energies between the silicene/five-layer substrate and silicene/"massive" substrate systems differ by no more than 1%. In both cases, the adhesion energies can be ordered as follows: $E_{adh}^{C} < E_{adh}^{Au} < E_{adh}^{Al} < E_{adh}^{Ag} < E_{adh}^{Cu} < E_{adh}^{Ni}$. Consequently, the lowest adhesion energy is observed in the silicene/graphite system (0.3 eV), while highest energy is observed in the silicene/nickel system (2.873 eV). The following regularity was obtained for the distance between the silicene and the substrates: $\Delta_{Si-Ni} < \Delta_{Si-Cu} < \Delta_{Si-Al} < \Delta_{Si-Ag} < \Delta_{Si-Au} < \Delta_{Si-C}$. Thus, the smallest distance was obtained between the silicene and the nickel substrate, and the largest between the silicene and the graphite substrate. The bond lengths for metal substrates correspond to those for cubic face-centric lattices of these materials [163].

Density functional theory (DFT) calculations from first principles make it possible to determine the Density of Electronic States (DOS) and the band structure. The DOS indicates the number of states that can be occupied by electrons in a material. DOS reflects these characteristics on a spectrum of energy levels. Based on DOS, many other physical properties of a material can be directly calculated, such as the effective mass of electrons in charge carriers, the electronic contribution to the heat capacity of metals, and the band gap of crystal structures. The band structure shows the allowable levels of the electronic energy of solid materials, i.e. it gives an idea of the energies of crystalline orbitals.

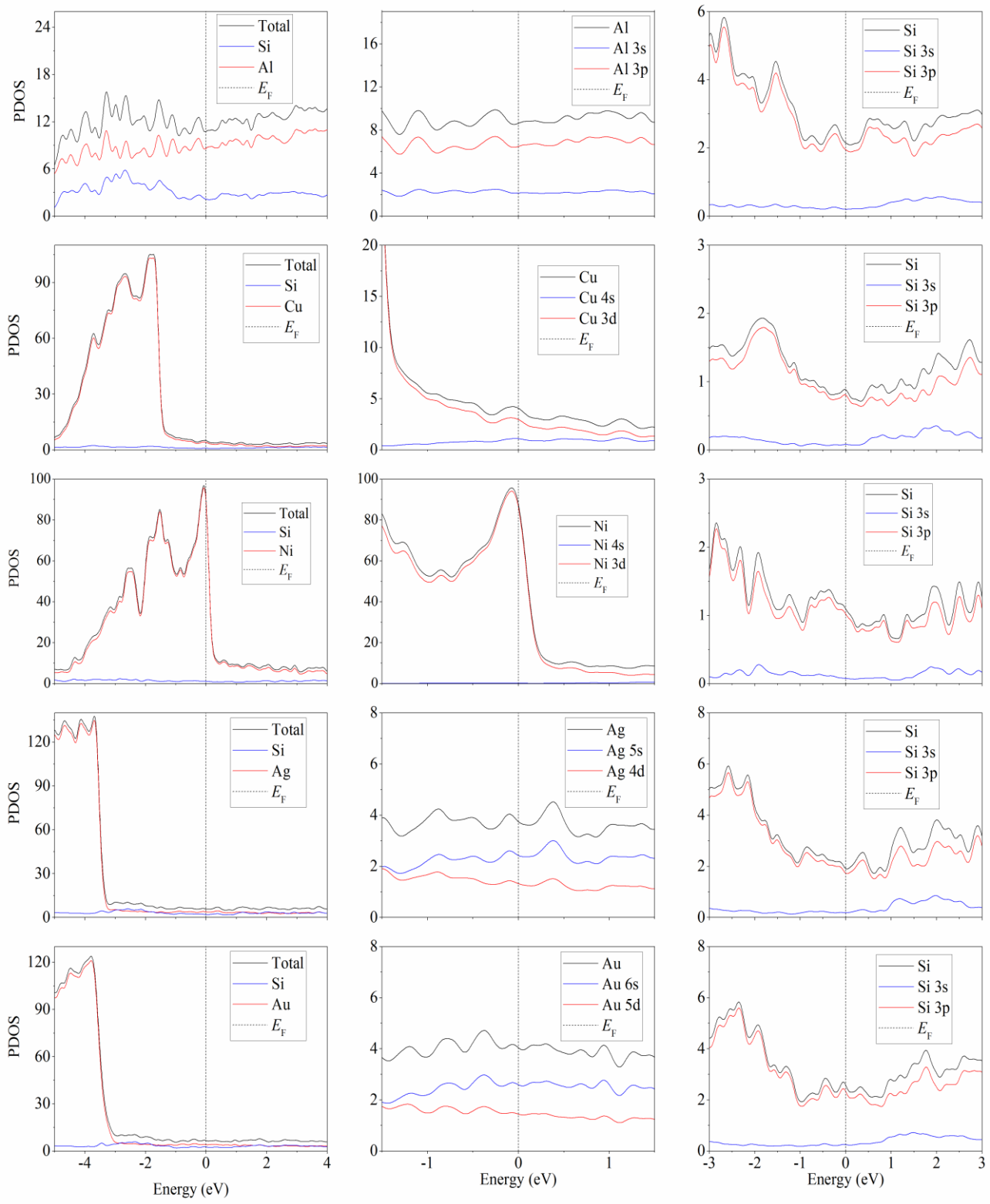

Figure 13 Partial spectra of electronic states of systems "silicene on «massive» aluminum, copper, nickel, silver and gold substrate".

The practical significance of the band structure lies in informing about the electrical properties of the material. In other words, the band structure determines whether the material is metallic, semi-metallic, or insulating. This two-dimensional representation of energies of the material with a band gap also provides information on the type of band gap (direct or indirect) as well as its magnitude.

The partial spectra of the electronic states of the systems “silicene on substrates with fixed z coordinates of the lower layer” are shown in Figure 13. In all systems without exception, silicene metallization occurs due to interaction with the substrate. In the case of silicene on copper, silver, and gold substrates, the 3p electrons of silicon interact with the s and d electrons of metals. While for silicene on a nickel substrate, the 3p electrons of silicon interact with the 3d electrons of nickel, while for silicene on an aluminum substrate, the interaction occurs between the 3p electrons of silicon and aluminum.

The band structure and partial spectra of the electronic states of the "silicene on a similar graphite substrate" system are shown in Figure 14. The finite (non-zero) value of the density of electronic states at the Fermi energy level indicates the system acquisition of electronic conductivity. Conductivity appears due to the interaction of 2p electrons of carbon with 3p electrons of silicon. In this case, the Dirac cone associated with the silicene subsystem in the band structure turns out to be elevated above the Fermi level, and the graphene Dirac cone is located below the Fermi level.

The appearance of electronic conductivity improves the physical properties of the silicene anode, because contributes to an increase in the speed of its charging.

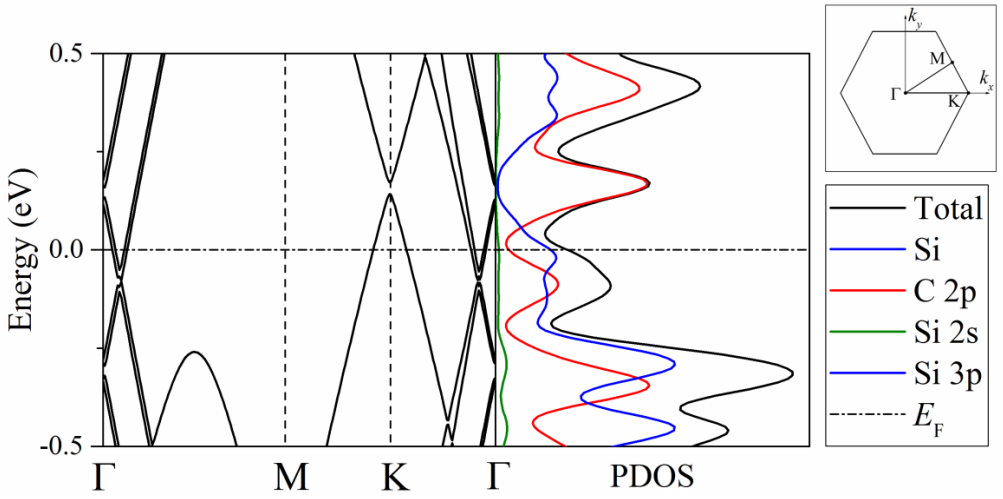

Figure 14 Band structure and partial spectra of electronic states of the "silicene on a «massive» graphite substrate" system, the Fermi level is shown by a horizontal dotted line; the inset shows the Brillouin zone with high symmetry points that determine directions in the band structure.

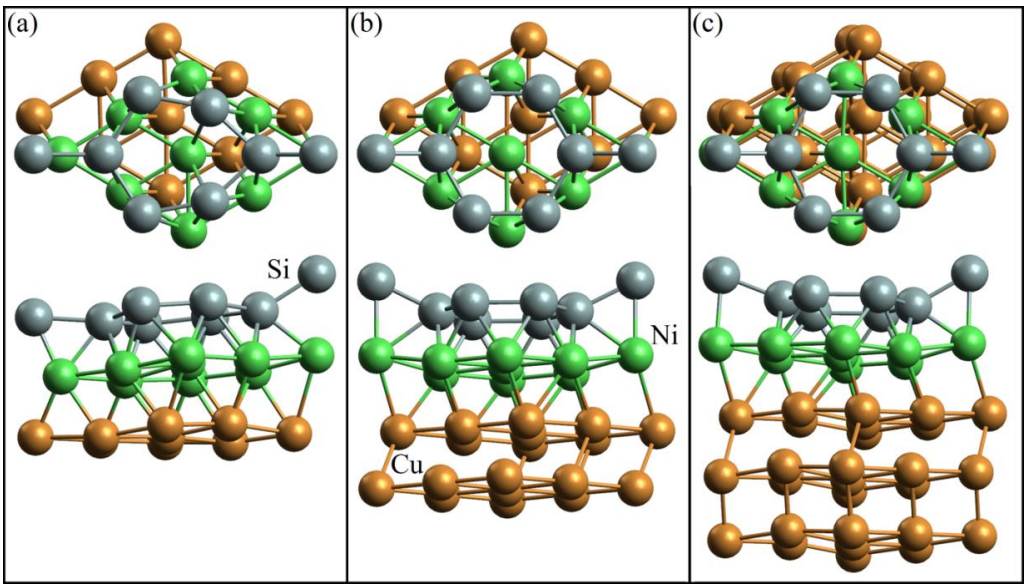

Figure 15 The geometric structure of silicene on (a) a single-layer, (b) two-layer and (c) three-layer copper substrate with an intermediate nickel layer between silicene and copper.

5.2 Copper substrate with an intermediate nickel layer

The most productive solar cells are made from high-purity (solar) silicon [164]. The metal contact with the solar cell can be made of copper coated with a thin layer of nickel to create a diffusion barrier [165]. Nickel facing Si forms nickel silicide, thereby reducing the contact resistance between the metal and Si [166]. Thus, three chemical elements (Si, Ni and Cu) are in close contact with each other. Determining the electronic properties of such a system is of considerable interest.

In [160], the silicene-copper substrate systems with an intermediate nickel layer between silicene and copper were studied based on quantum mechanical calculations. The initial systems were created by replacing the upper layer of the copper substrate with one layer of nickel (with a copper substrate thickness of 2–4 layers). The geometric structure of silicene systems on a copper substrate of various thicknesses with an intermediate nickel layer is shown in Figure 15.

The adhesion energy $E_{\text{adh}}^{\text{Cu-Ni}}$ between the nickel layer and the copper substrate was calculated as

$$E_{adh}^{\text{Cu-Ni}} = -\frac{E_{\text{tot}} - E_{\text{SiNi}} - E_{\text{Cu}}}{N_{\text{cel}}}, \qquad (9)$$

where E_{SiNi} and E_{Cu} are the total energies calculated for the silicene-nickel subsystem and copper substrate, respectively, and N_{cel} is the number of silicene unit cells.

Some characteristics of the considered systems are shown in Table 4. Among them, the adhesion energy between silicene sheet and copper substrate with an intermediate layer of nickel ($E_{adh}^{\text{Si-Ni}}$); adhesion energy between the copper substrate and the nickel layer ($E_{adh}^{\text{Cu-Ni}}$); binding energies between silicon atoms in a silicene sheet (E_b^{Si}); total Voronoi charge calculated for nickel (Q_V^{Ni}), copper (Q_V^{Cu}) and silicene (Q_V^{Si}).

Note that the distance between the silicene sheet and the intermediate nickel layer decreases from 1.890 to 1.795Å as the number of copper layers in the substrate increases from 1 to 3. In this case, the adhesion energy between nickel and copper increases from 2.356 to 2.889eV. The shortening of the Si–Ni distance is the strong adhesion of silicene to nickel, which is ~6% more than that to copper [30]. In addition, regardless of the thickness of the substrate, the nickel intermediate layer has an average negative charge of -1.114 a.u, which is compensated by the positive charges of the copper part of the substrate and silicene.

Table 4 – Energy characteristics* of systems silicene-copper substrate with an intermediate layer of nickel

N_{Cu}	E_{adh}^{Si-Ni}, eV	E_{adh}^{Cu-Ni}, eV	E_b^{Si}, eV	Q_V^{Ni}, eV.	Q_V^{Cu}, a.u.	Q_V^{Si}, a.u.
1	3.647	2.356	4.563	-1.058	0.676	0.382
2	3.449	2.725	4.615	-1.197	0.859	0.335
3	3.452	2.889	4.595	-1.089	0.705	0.379

*Parameter designations are described in the text.

5.3 Graphene, boron nitride, and silicon carbide substrates

In [29], the adsorption behavior of the lithium (sodium) atom was studied for the silicene/graphene (Si/G) heterostructure. The concentration of deposit Li or Na atoms did not exceed x = 1.375. At all considered concentrations of Li and Na, negative binding energies of these metals with the Si/G substrate were obtained. Adsorption for Na has always been weaker than for Li. However, even when the surface was completely filled with alkali metals, their binding energy with the surface remained quite low (below 0.65 eV for Li and below 0.55 eV for Na). It can be assumed that, due to strong adsorption, lithium and sodium atoms can be effectively fixed on the surface of the Si/G heterostructure, even at high concentrations of them, and clustering will not occur during discharge/charging. According to estimates, at the highest concentration of lithium and sodium achieved here, the capacity of the anode created from the Si/G heterostructure will be 487 mAh g^{-1}. In this case, the outer surface of the

silicene and the interlayer space between silicene and graphene should be completely adsorbed by lithium or sodium atoms. In this case, the interlayer distance in silicene will increase by approximately 20% upon lithium intercalation, and by 40% upon filling the anode with sodium. This estimate of the negative electrode capacitance appears to be underestimated compared to other literature data [36–38] due to the low lithium concentrations realized in [29].

Among the nonmetallic substrates for silicene, graphene, two-dimensional boron nitride, and one-, two-, and three-layer two-dimensional silicon carbide were studied by DFT calculations [167]. The adhesion energy of silicene with two-dimensional nanomaterials was calculated according to the expression:

$$E_{adh}^{\mathrm{Si-2d}} = -\frac{E_{\mathrm{tot}} - E_{\mathrm{Si}} - E_{\mathrm{2d}}}{N_{\mathrm{cel}}}, \quad (10)$$

where E_{tot} is the total energy of the "silicene-two-dimensional nanomaterial" system, E_{Si}, E_{2d} are the total energies calculated for the silicene sheet and two-dimensional nanomaterial, respectively.

Some metric and energy properties of the systems "silicene - two-dimensional material" are presented in Table 5. Among them: $L_{(Si\text{-}Si)}$ is Si-Si bond length in a silicene sheet; $\Delta_{(Si\text{-}Si)}$ is the distance between silicene sublattices; $\Delta_{(Si\text{-}2d)}$ is the distance between the silicene sheet and the two-dimensional material; E_b^{Si} is the binding energy between silicon atoms in a silicene sheet; $E_{adh}^{\mathrm{Si-2d}}$ is the adhesion energy between the silicene sheet and the two-dimensional material; Q_V^{Si} is the total Voronoi charge of the silicon atoms of the silicene sheet; BG is the width of the direct (d) or indirect (i) band gap of the combined nanomaterial.

The lowest adhesion energy of 0.235 eV is observed when silicene is in contact with two-dimensional boron nitride. When silicene is on graphene or single-layer silicon carbide, the adhesion energy is higher by 20.8 and 16.6%, respectively. An increase in the number of layers in two-dimensional silicon carbide from one to three leads to a significant increase (more than 6 times) in the adhesion energy due to the onset of the SiC transition from a two-dimensional to a bulk state (Figure 16). During the formation of heterostructures, the total charge is redistributed between original nanomaterials and p-n junctions are formed. Thus, in the cases of silicene on graphene and silicene on 2D boron nitride, the silicene sheet acquires a negative charge of -0.214 and -0.062a.u., respectively. Silicene on single-layer silicon carbide remains virtually electro-neutral. However, the addition of the second and third layers of silicon carbide leads to an increase in the positive net charge of the Si atoms in the silicene sheet.

Fragments of two-layer configurations composed of silicene, as well as silicene and other layers (two-dimensional silicon carbide, graphene and boron nitride) are shown in Figure 17. The closest approach is observed between the silicene sheets, while the largest gap is formed between the single-layer silicon carbide and the silicene sheet.

Figure 18 shows the band structures and electron density of state spectra of two-layer silicene, silicene on 2D silicon carbide, silicene on graphene, and silicene on boron nitride. It can be seen that in the two-layer silicene and combined nanomaterials "silicene-boron nitride", "silicene-two-dimensional silicon carbide" semiconductor properties are preserved. If the band gap in single-layer silicene was 0.027 eV [168], then in two-layer silicene, it expands to 0.265 eV; however, the Dirac cones are not preserved, in contrast to the Si-2dSiC and Si-BN systems.

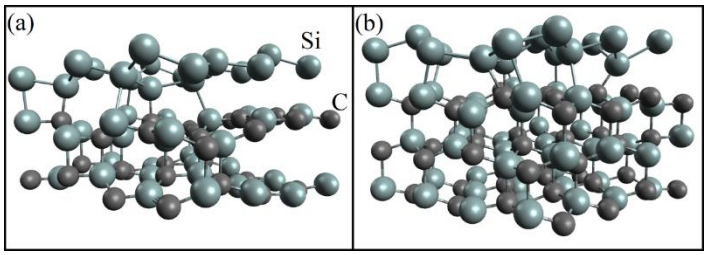

Figure 16 Configuration of the system "silicene on (a) two-layer and (b) three-layer two-dimensional silicon carbide" after geometric optimization.

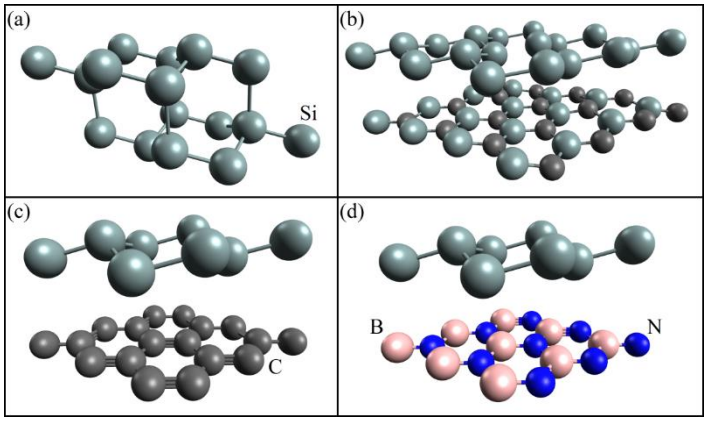

Figure 17 Configurations of two-layer systems: (a) two-layer silicene, (b) silicene on two-dimensional silicon carbide, (c)

silicene on graphene, and (d) silicene on boron nitride - after geometric optimization.

Table 5 – Metric and energy properties* of "silicene-2d material" systems

2d	$L_{(Si\text{-}Si)}$, *Å*	$\Delta_{(Si\text{-}Si)}$, *Å*	$\Delta_{(Si\text{-}2d)}$, *Å*	E_b^{Si}, *eV*	E_{adh}^{Si-2d}, *eV*	Q_V^{Si}, *a.u.*	*BG, eV*
Si	2.330	0.843	2.080	6.394	0.725	-	0.265 (i)
G	2.282	0.638	3.611	4.312	0.284	-0.214	M
1 SiC	2.398	0.487	3.677	4.323	0.274	0.020	0.047 (d)
2 SiC	2.436	0.875	2.728	4.216	1.148	0.252	0.078 (d)
3 SiC	2.475	0.868	2.596	4.160	1.771	0.448	0.017 (i)
BN	2.288	0.612	3.633	5.057	0.235	-0.062	0.012(d)

*Parameter designations are described in the text.

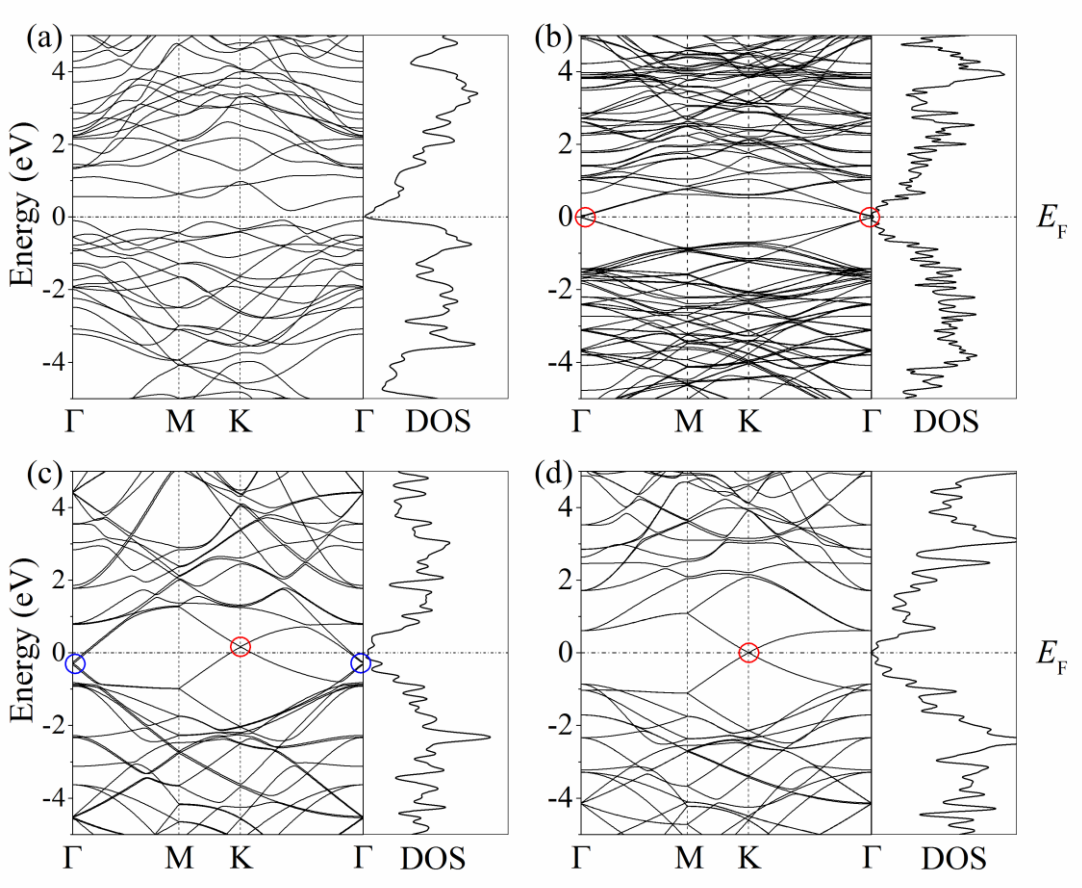

Figure 18. Band structures and electron state density spectra of two-layer systems: (a) two-layer silicene, (b) silicene on two-dimensional silicon carbide, (c) silicene on graphene, and (d) silicene on boron nitride; the red circle shows the top of the Dirac cone for silicene, and the blue circle is that for graphene.

The interaction between silicene and graphene leads to the appearance of conductive properties while maintaining the silicene and graphene Dirac cones. The vertices of the Dirac cone for silicene are at different points of high symmetry when silicene is placed on graphene (Figure 18b, point Γ) and on silicon carbide (Figure 18c, point K). This is due to the use of different superlattices for silicene: a 2×2 superlattice was used on graphene, and a 3×3 superlattice was used on silicon carbide. Such superlattices were installed for better compatibility with substrate superlattices (3×3 for graphene and 4×4 for SiC). Figure 18c shows that the silicene Dirac cone (point K) shifts above the Fermi level, while the graphene Dirac cone (point Γ) shifts below the Fermi level.

Band structures and spectra of the density of electronic states of combined nanomaterials of silicene in combination with two- and three-layer two-dimensional silicon carbide are shown in Figure 19. It can be seen that the resulting combined nanomaterials remain semiconductors, but the Dirac cones are not preserved.

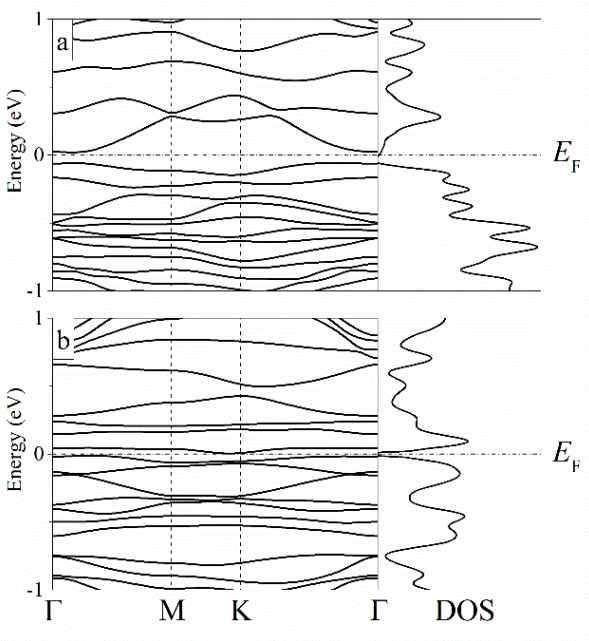

Figure 19 Band structures and electron state density spectra of silicene on (a) two-layer and (b) three-layer two-dimensional silicon carbide.

5.4 Simulation of nuclear transmutation doping of silicene with phosphorus

In [169], on the basis of DFT simulation, mono- and bilayers of silicene on a graphite substrate subjected to NTD were studied. In this case, some of the silicon atoms were replaced by phosphorus atoms, and some of the carbon atoms were replaced by nitrogen atoms. The replacement of Si by P was carried out in all possible positions of Si atoms in silicene. The replacement of C atoms by N was carried out only in the upper sheet of graphene. The band structures and spectra of the electronic state were calculated.

Geometric optimization produced significant changes in the structure of the doped Si/C system (Figure 20). Structural rearrangement resulted in an increase in the average distance between the silicene sublattices, which changed from 0.44 to 0.56 Å and from 0.44 to 1.01 Å for single-layer and double-layer silicene, respectively.

The projections of the densities of states of the Si/C system, depending on its modification by phosphorus and nitrogen atoms, are shown in Figure 21. All systems on a carbon substrate acquire conductive properties. The number and arrangement of phosphorus atoms in the silicene sheet and nitrogen atoms in the carbon substrate only affect the degree of "metallization".

Similar the projected densities of states obtained for the bilayer silicene on a carbon substrate are shown in Figure 22. Replacing 1-2 C atoms in the graphite substrate with N atoms results in a Fermi level shift. In this case, the conductivity at the p-level of carbon increases. Low conductivity at a band gap of 8 to 18 meV is observed in the absence of N atoms in the carbon substrate and is determined by the position of P atoms in silicene. The bilayer silicene system acquires semiconductor properties when two Si atoms are replaced by P atoms. The following configurations correspond to this situation: 1) both atoms are in the lower sublattice of the lower silicene sheet; 2) both atoms are localized in the upper sublattice of the lower silicene layer; 3) one atom is located in the lower, and the other – in the upper sublattice of the lower sheet of silicene; 4) one atom

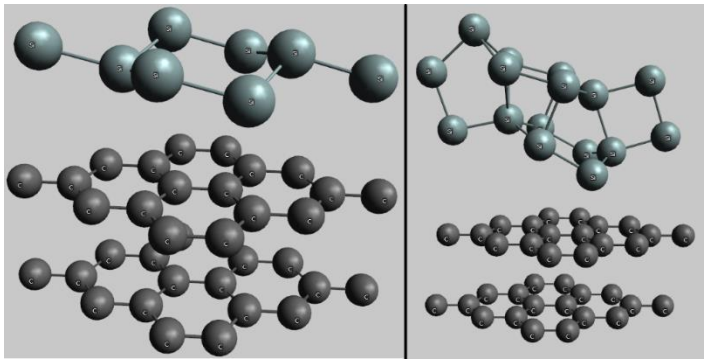

Figure 20 Unmodified single layer silicene on a graphite substrate (left) and a similar two layer silicene after geometric optimization (right).

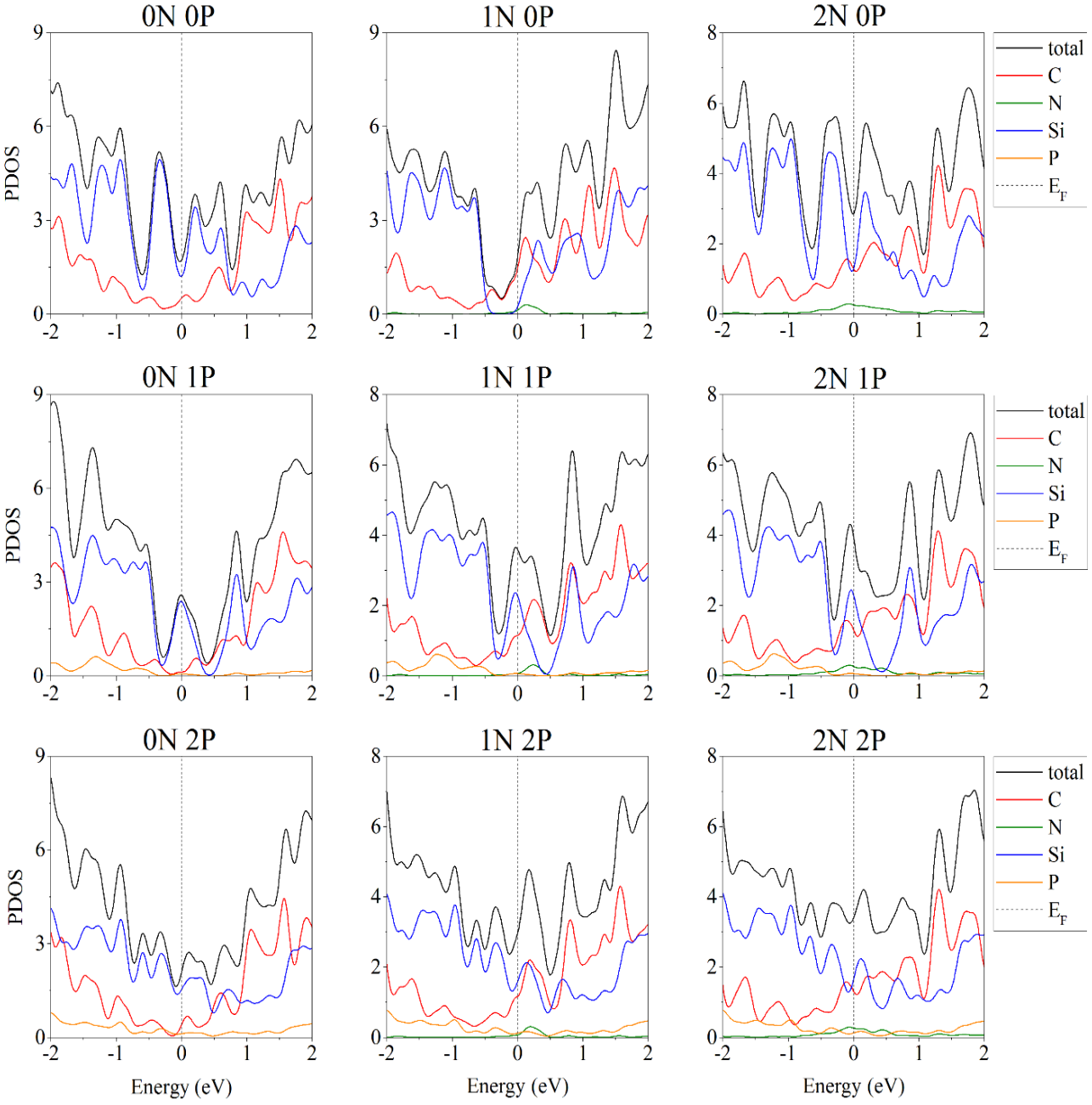

Figure 21 Projected densities of states of modified «monolayer silicene/C» systems in which a silicene sheet contains from 0 to 2 P atoms, and a graphite substrate contains from 0 to 2 N atoms.

belongs to the lower sublattice of the lower layer, and the other atom belongs to the lower sublattice of the upper layer of silicene. Note that the PDOS shapes for configurations 2 and 3 are almost identical and differ only in the band gap.

Thus, the Si/C system subjected to the NTD procedure retains the conductive properties acquired by silicene placed on a graphite substrate. A noticeable deterioration in the electronic conductivity can occur only in unlikely cases, when only the silicon part of the system is doped. An increase in the electronic conductivity of the anode is a positive factor for the functioning of the LIB.

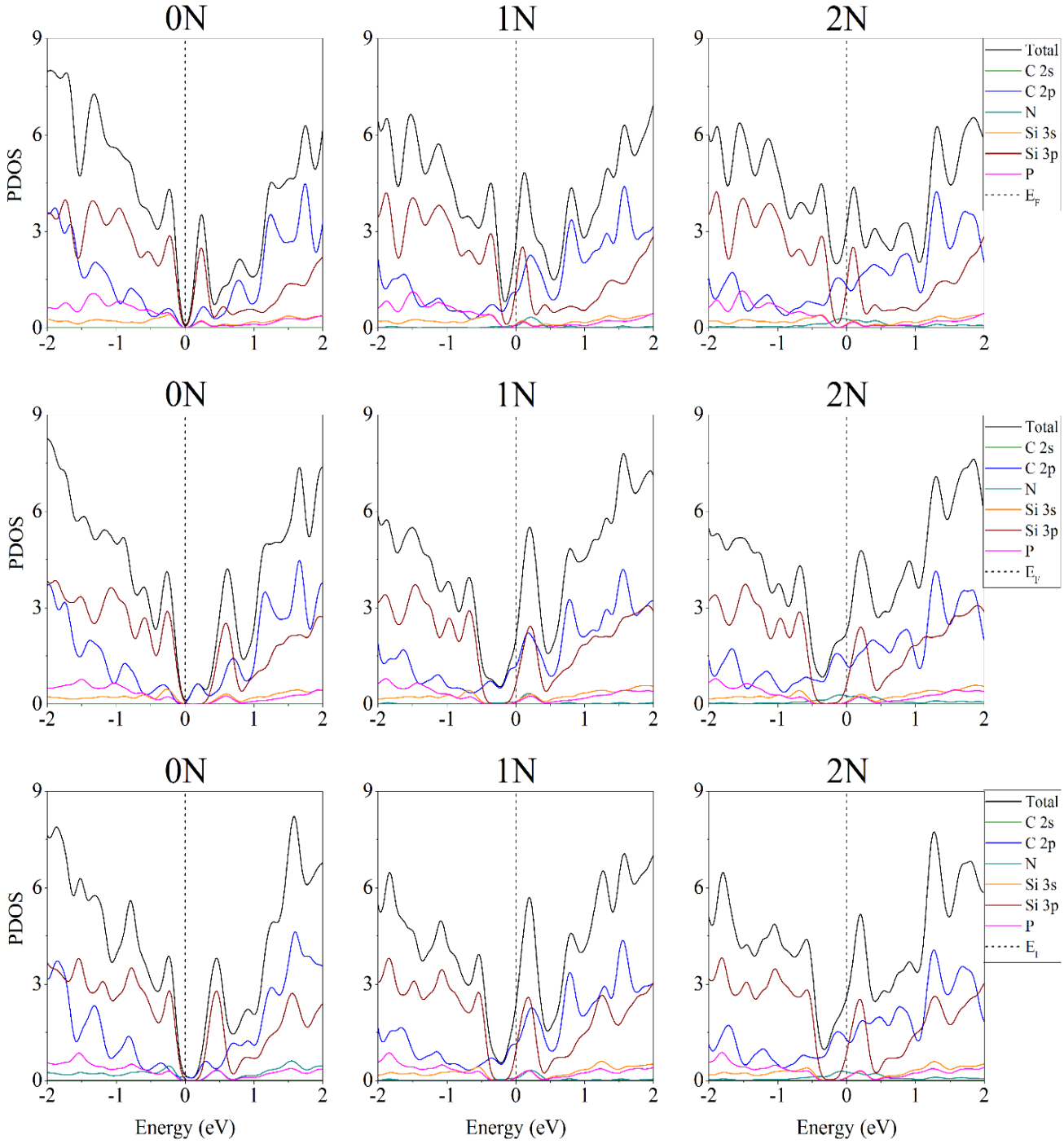

Figure 22. Projected densities of states of modified systems of «bilayer silicene/C» in which a silicene sheet contains 2 P atoms, and a graphite substrate contains from 0 to 2 N atoms.

6. Discussion

6.1 Features of the existence of silicene and the prospects for its use

So far, the growth of Si honeycomb structures has been recorded on a limited number of substrates such as Ag, Au, Ir, ZrB_2 and MoS_2, and DFT calculations combined with experimental observations indicate that all obtained two-dimensional silicon superstructures deviate from the structure of free-standing silicene. [88, 97, 131, 136, 170–174]. Among them, superlattices obtained on Ag(111) and ZrB_2(0001) are of particular interest, since the observed electronic spectra for them can be easily explained on the basis of the theoretical concept of silicene. Epitaxial conditions, type and degree of buckling of silicene can vary, which in turn affects the electronic properties. The close relationship between structure and electronic properties makes the atomic scale of the height of bends on the surface a highly significant parameter in the description of silicene. On the other hand, the structural flexibility associated with mixing sp^2 and sp^3 hybridizations may allow the design of desired properties, such as the presence of a bandgap, which is difficult to achieve in pure sp^2 hybridized graphene [171]. The behavior of silicene growth on the Ag(111) surface strongly depends on temperature and a number of other factors [88, 97, 136, 141, 170, 172]. Among the presented superstructures, subsequent annealing cannot make a transition from one observed phase to another [170]; therefore, there is an unnegligible energy barrier between these phases.

Calculations by the density functional theory showed that there are no true covalent bonds between the Si layer and the Ag substrate [175]. However, as the silicene and Ag substrates approach each other significantly, the electron densities of the closest atoms of these materials overlap. The localized accumulation of electrons at the interface indicates a weak chemical interaction between silicene and the first Ag layer. The existence of a chemical interaction between the Si layer and the Ag surface is consistent with the hybridization effects considered in [176, 177]. At the same time, the interaction between the upper Si atoms and the surface Ag atoms differs significantly from the interaction between the lower Si atoms and the Ag substrate. Electrons flow from the Si atoms to the Ag substrate, so that the upper Si layer is positively charged, while the first Ag plane carries a negative charge. Hence, we can conclude that an electrostatic interaction occurs between the upper Si atoms and the flat Ag surface. As a result of such an interaction, a loss of stability of the hexagonally structured Si layer can be observed. Thus, silicene located on the Ag(111) surface binds to the substrate both due to the accumulation of charge density at the interface and via electrostatic interaction. Weak chemisorption of silicene on an Ag substrate was also observed in [178]. As a result of the loss of electrons from the upper Si atoms (0.13 e^- per one Si atom), the reactivity of silicene on the Ag(111) surface turns out to be lower than for suspended silicene. Ab initio calculations show that a free standing silicene can form a covalent bond with hydrogen and NO_2, as well as an ionic bond with halogens [179–181].

A significant number of works have been devoted to the study of monolayer silicene [182–185]. At the same time, multilayer silicene is far from sufficient studied. Separate two-layer silicene was considered in [186–189], but the mechanism that determines the relative stability of the obtained phases was not determined. In addition, two-layer silicene can be both a metal and a semiconductor, depending on the method of stacking silicene sheets [187–189]. Si surfaces seem to be a convenient material for the manufacture of electronic devices. A certain similarity between multilayer silicene and atomic layers of a massive silicon crystal parallel to the Si (111) plane is intriguing. In fact, the split Si(111) surface has a 2×1 periodicity, but after annealing it transforms into a more stable 7×7 superlattice. The 2×1 phase is identified as a π-bonded chain structure [190]. For the 7×7 phase [191, 192], a "dimer-adatom" stacking fault model was presented [193, 194]. The evolution in the reconstruction of the surface phases of multilayer Si is not yet clear. Most of the solar cells currently being manufactured are based on three-dimensional (3D) Si. However, 3D-Si is not an ideal material for optoelectronic applications due to the relatively large direct band gap [195]. The discovery of multilayer silicene materials with excellent optoelectronic properties could provide a breakthrough in the technology of future optoelectronics.

For a long time, the implementation of the epitaxial synthesis of reconstructed multilayer silicene conserving

Dirac fermions seemed to be an impossible task. Nevertheless, multilayer silicene was obtained. In [196], using complex X-ray crystallography, it was demonstrated that the preparation of multilayer silicene requires fairly low growth temperatures (~200 °C), while the three-dimensional growth of silicon crystallites occurs at higher temperatures (~300 °C). The temperature-induced transition to obtaining bulk silicon partly explains the various experimental data and smooths out their contradictory interpretation.

Bilayer silicene does not tend to undergo irreversible structural changes during lithiation and delithiation cycles. The relief geometry of silicene can be formed during the drift of the Li^+ ion between its sheets. In addition to mixing sp^2 and sp^3 hybridizations, a possible effect of the relief geometry of silicene is the establishment of a Dirac-type electron dispersion. The abundance of Si, its rare ability to retain Li, the flexibility of atomic layers, and the low energy barrier to diffusion of Li^+ ions make it attractive to use silicene in lithium-ion batteries. With it, a high energy density can be created and the life cycle of the battery can be improved. Doping of two-layer silicene with bromine or hydrogen leads to the appearance of anti- or ferromagnetism at room temperature [197]. Consequently, new opportunities appear for creating high-performance electronic devices based on the use of two-layer silicene.

The area of potential application of silicene continues to expand. The natural abundance of Na resources and their relative cheapness make Na-ion batteries a promising candidate for replacing lithium-ion batteries on a large scale. In this regard, silicene retains a high potential for use as an anode in sodium-ion batteries. In this context, stand-alone silicene, graphene-silicene-graphene heterostructures, and graphene-silicene superlattices can be applied in Na-ion batteries [198]. Estimated capacities of Na batteries using stand-alone silicene and graphene-silicene superlattices for the anode are ~950 mAh/g and 730 mAh/g, respectively. Therefore, such anodes appear to be highly competitive with graphite anodes having a theoretical power of 372 mAh/g. In addition, diffusion barriers in sodium electrodes are expected to be less than 0.3 eV.

The structure of silicene can be modified by introducing -C≡C- inserts (parts of acetylene) into all Si-Si bonds [199]. This so-called c-silicyne (c-silicyne) has a flat optimized structure, i.e. acquires the morphology of graphene. C-silicine has a zero band gap and semi-metallic behavior in the non-magnetic state, but becomes a semiconductor in the anti-ferromagnetic state. Tensile deformation makes it possible to strengthen and even linearly increase the antiferromagnetism in c-silicyne. The heterostructure obtained by applying a stressed c-silicyne sheet to a MoS_2 monolayer can be a promising material for high power solar cells with a conversion efficiency in excess of 20%. C-silicine nanoribbons and nanosheets have unique electronic and magnetic properties that have a variety of potential applications.

Graphene substrate for silicene is significantly preferred over a metal one. Unlike metal substrates, the interaction between silicene and graphene is mainly of the van der Waals type, which creates conditions for maintaining the intrinsic properties of silicene. Moreover, the incorporation of graphene provides better mechanical properties and higher electronic conductivity, while also protecting silicene from damaging environmental influences. First-principles calculations show that silicene/graphene heterostructures not only retain high capacitance and low energy migration barriers for both lithium and sodium, but also provide stronger adsorption, better mechanical rigidity, and structural stability in charge/discharge cycles compared to a free-standing silicene [29].

Such heterostructures are attractive for use as the anode of lithium/sodium-ion batteries. However, the calculations performed on the basis of DFT in [29] extremely idealize the situation. This is due not only to the very small size of the system (consisting of 16 Si atoms and 36 C atoms) and the highly limited time of MD calculations performed from first principles. In [29], first-principles calculations using generalized gradient approximation were applied to study the adsorption and diffusion of lithium and sodium atoms on silicene, graphene, and a silicene/graphene composite. Both processes have been studied exclusively by calculating the energy characteristics. No direct calculation of the diffusion coefficients was carried out. The initial positions of the Li and Na atoms were determined in advance. The energy characteristics also served as a source of information for determining the direction of diffusion.

6.2 Benefits of using silicene anode

To date, graphite has remained the preferred anode material, including LIBs operating in Li salt/organic

liquid electrolytes. These batteries suffer from excess consumption of Li^+, which is associated with the formation of the solid electrolyte interface (SEI). The main share of SEI education falls on the first cycle. Outwardly, it manifests itself in an almost 10% loss in the capacity of graphite anodes. SEI accumulates during the further operation of the battery, i.e. the thickness of this film increases due to the inclusion of an increasing amount of Li^+ in it. The SEI film creates electronic isolation and prevents Li^+ intercalation. As a result, the achievable energy and power density LIB are limited. Due to the expansion and contraction of the graphite lattice during cycling, the SEI layer exhibit instability. The loss of lithium ions from the electrolyte and the unstable behavior of SEI lead to degradation of LIB [200–202].

It is widely believed that the higher capacity of the silicon anode is achieved due to the formation of an alloy of lithium with silicon [203]. The alloying reaction is represented as [204]

$$Si + 4.4\ Li^+ + 4.4\ e^- \leftrightarrow Li_{4.4}Si$$

Silicon is characterized as the champion in theoretical capacity among all anode materials (second only to hydrogen). However, during lithiation, the volume of the silicon electrode increases greatly. This causes strong stresses inside the material, which can lead to crushing of the electrode material and its separation from the collector [205]. The tearing SEI film requires a new consumption of lithium for its recovery. The efficiency of LIB cycling with a silicon anode is low [206, 207]. The use of thin silicon films, as well as porous silicon, significantly reduces the stress caused by the change in the volume of silicon anodes [208].

The use of silicene as an anode material has its advantages and disadvantages. Silicene can withstand large deformations (> 0.15) with armchair, zigzag and biaxial deformation [209]. The second-order elastic constants and in-plane Young's modulus also indicate that silicene is mechanically stable. The mechanical properties of silicene demonstrate isotropic behavior: both in the "zigzag" and "armchair" directions, the Young's modulus of silicene is close to 199.3 GPa, and the Poisson's ratio is 0.17 [210]. According to [211], silicon is not an elastically isotropic material. The values of Young's modulus and Poisson's ratio for it are 140–180 GPa and 0.265–0.275, respectively.

However, silicene has a very low thermal conductivity. Therefore, in order to remove heat from the silicene contained in the electrochemical device, it is necessary to contact the silicene with a highly thermally conductive material, such as a metal. The thermal transfer in silicene is dominated by longitudinal phonon modes [212]. Restricting the free path of phonons reduces the thermal conductivity. The use of silicene in combination with silicon carbide does not increase the thermal conductivity of the material. The thermal conductivity of SiC phononic crystals is 30–40% lower than that of silicene [213]. With an increase in the concentration of vacancies in SiC crystals or an increase in temperature, a significant decrease in thermal conductivity is observed [214]. Limited thermal conductivity of graphene-filled materials in the direction not aligned with graphene alignment is also an obstacle to the use of silicene/graphene anode material. The inherent semimetallicity of both components (graphene and silicene) largely limits their use in functional devices.

The demand for lithium-ion batteries continues to increase. In this regard, and with an increase in the price of lithium, there is a growing interest in Na^+, K^+, Mg^{2+} and others, which can be obtained at a lower price. There is an urgent need to optimize electrochemical devices, including through the introduction of new efficient anode materials [215].

Undoubtedly, an understanding of the physical processes that occur with Li^+ ions and other alkali metal ions in the atomic scale is a necessary condition for the development of more efficient batteries. The widely used lithium-ion batteries are easy to maintain, but still not safe. Thus, a catastrophic failure of lithium-ion batteries was observed in the automotive industry and in aviation [216]. Perhaps this is due to the imperfection of modern technologies [214, 215].

The charge carriers in batteries are usually lithium and sodium. Lithium has a higher gravimetric capacity. However, there is much more sodium in nature. Therefore, sodium is a cheap material for LIBs, especially for their stationary version [112]. Lithium-, sodium-, and potassium-ion batteries were compared in detail in [219–223].

First-principle modeling has been widely used to study the lithiation of silicon-based nanomaterials for LIB anodes. However, there is still a lack of fundamental research on the formation and growth of SEI layers. The

combination of computational and experimental research will be critical to create the next generation of LIBs with a long service life at an affordable cost.

7. Conclusions

In this review is the fundamental idea that the structure of 2D materials largely determines their properties. To date, extensive theoretical conclusions have been made about the properties of 2D materials, for which there is no experimental verification. Only a few properties of 2D materials have been measured in selected cases. For example, the stiffness and tensile strength of quasi-freely suspended graphene have been measured by atomic force microscopy nanoindentation. There are problems not only in the preparation of suspended monolayers, but also in the interpretation of experimental data based on simple mechanical models. Changes in the mechanical properties of monolayers due to interaction with substrates during fabrication, handling, and operation are still not well understood. This is especially true for covalent and ionic interactions, which can change the bond length and bond energy. Such interactions cause changes in fundamental mechanical and electronic properties.

The use of new 2D anode materials for next-generation metal-ion batteries aims to achieve higher energy density, better battery performance, and stable cycle characteristics. The problem of achieving high safety of an electrochemical device and its low cost is still important for the solution. The goal can be achieved through the use of silicon-containing materials, including in the form of two-dimensional heterogeneous structures. The effective surface area of the electrode can be increased by structural modification of the material. As a consequence, the first reversible capacity of the anode material can be improved. An improvement in the Coulomb efficiency can be achieved by increasing the electronic conductivity of the material, for example by heteroatomic doping. Based on the combination of silicene with graphene, it is possible to form a layered, extremely flexible and strong material with high electronic conductivity and chemical stability in the electrolyte. However, the addition of graphene leads to a decrease in the electrode capacitance. It is possible that the replacement of graphene in the heterostructure with other 2D materials or the creation of more complex silicon-containing and including graphene heterostructures will help to obtain higher battery performance.

Acknowledgements

This work is executed in the frame of the scientific theme of Institute of High-Temperature Electrochemistry UB RAS, number FUME-2022-0005, registration number 122020100205-5.

Conflict of interest

The authors declare no conflict of interest.

References

1. Pang J, Bachmatiuk A, Yin Y, Trzebicka B, Zhao L, Fu L, Mendes RG, Gemming T, Liu Z, Rummeli MH, Applications of phosphorene and black phosphorus in energy conversion and storage devices. Adv. Energy Mater. **8** (2017) 1702093.
2. Adams RA, Mistry AN, Mukherjee PP, Pol VG, Materials by design: Tailored morphology and structures of carbon anodes for enhanced battery safety. ACS Appl. Mater. Interfaces, **11** (2019) 13334–13342.
3. Wang L, Wang Z, Sun Y, Liang X, Xiang H, Sb2O3 modified PVDF-CTFE electrospun fibrous membrane as a safe lithium-ion battery separator. J. Membr. Sci. **572** (2019) 512–519.
4. Galashev AY, Computational investigation of silicene/nickel anode for lithium-ion battery. Solid State Ionics, **357** (2020) 115463.
5. Su X, Wu Q, Li J, Xiao X, Lott A, Lu W, Sheldon BW, Wu J, Silicon-based nanomaterials for lithium-ion batteries: a review. Adv. Energy Mater. **4** (2013) 375–379.
6. Liu L, Lyu J, Li T, Zhao T, Well-constructed silicon-based materials as high-performance lithium-ion battery anodes. Nanoscale, **8** (2016) 701–722.
7. Du FH, Wang KX, Chen JS, Strategies to succeed in improving the lithium-ion storage properties of silicon nanomaterials. J. Mater. Chem. A, **4** (2016) 32–50.
8. Favors Z, Wang W, Bay HH, George A, Ozkan M, Ozkan C, Stable cycling of SiO2 nanotubes as high-performance anodes for lithium-ion batteries. Sci. Rep. **4** (2014) 4605.
9. Miyachi M, Yamamoto H, Kawai H, Ohta T, Shirakata M, Analysis of SiO anodes for lithium-ion batteries. J. Electrochem. Soc. **152** (2005) A2089.
10. Yao Y, Zhang JJ, Xue LG, T. Huang T, Yu A, Carbon-coated SiO2 nanoparticles as anode material for lithium ion batteries. J. Power Sources. **196** (2011) 10240–10243.
11. Yan N, Wang F, Zhong H, Li Y, Wang Y, Hu L, Chen Q, Hollow porous SiO2 nanocubes towards high-performance anodes for lithium-ion batteries. Sci. Rep. **3** (2013) 1568.
12. Zhang YF, Li YJ, Wang ZY, Zhao K, Lithiation of SiO2 in Li-ion batteries: In situ transmission electron microscopy experiments and theoretical studies. Nano Lett. **14** (2014) 7161–7170.

13. Gil M, Rabanal ME, Varez A, Kuhn A, Garcia-Alvarado F, Mechanical grinding of Si3N4 to Be used as an electrode in lithium batteries. Mater. Lett. **57** (2003) 3063–3069.
14. Ahn D, Kim C, Lee J, Park B, The effect of nitrogen on the cycling performance in thin-film SiI-xNx anode. J. Solid State Chem. **181** (2008) 2139–2142.
15. Yang J, Guzman RC, Salley SO, Simon KY, Chen B, Cheng MM, Plasma enhanced chemical vapor deposition silicon nitride for a high-performance lithium ion battery anode. J. Power Sources. **269** (2014) 520–525.
16. Wu CY, Chang CC, Duh JG, Silicon nitride coated silicon thin film on three dimensions current collector for lithium ion battery anode. J. Power Sources **325** (2016) 64–70.
17. Suzuki N, Cervera RB, Ohnishi T, Takada K, Silicon nitride thin film electrode for lithium-ion batteries. J. Power Sources. **231** (2013) 186–189.
18. Yi R, Dai F, Gordin ML, Chen S, Wang D, Micro-sized Si–C composite with interconnected nanoscale building blocks as high-performance anodes for practical application in lithium-ion batteries. Adv. Energy Mater. **3** (2013) 295–300.
19. Chang XH, Li W, Yang JF, Xu L, Zheng J, Li XG, Direct plasma deposition of amorphous Si/C nanocomposites as high performance anodes for lithium ion batteries, J. Mater. Chem. A **3** (2015) 3522–3528.
20. Hsieh C-C, Liu W-R, Carbon-coated Si particles binding with few-layered graphene via a liquid exfoliation process as potential anode materials for lithium-ion batteries. Surf. Coatings Technol. **387** (2020) 125553.
21. Kumari TS, Jeyakumar D, Kumar TP, Nano silicon carbide: A new lithium-insertion anode material on the horizon. RSC Adv. **3** (2013) 15028–15034.
22. Zhang HT, Xu H, Nano crystalline silicon carbide thin film electrodes for lithium-ion batteries. Solid State Ionics **263** (2014) 23–26.
23. Lu Z, Wong T, Ng TW, Wang C, Facile synthesis of carbon decorated silicon nanotube arrays as anode material for high-performance lithium-ion batteries. RSC Adv. **4** (2014) 2440–2446.
24. Lv Y, Wu Z, Fang Y, Qian X, Asiri AM, Tu B, Zhao D, Hierarchical mesoporous/microporous carbon with graphitized frameworks for high-performance lithium-ion batteries. APL Mater. **2** (2014) 366–377.
25. Qian J, Ma J., He W., Hua D. Facile synthesis of prussian blue derivate-modified mesoporous material via photoinitiated thiol-ene click reaction for cesium adsorption. Chem. Asian. J. **10** (2015) 1738–1744.
26. Liu X, Zhu X, Pan D, Solutions for the problems of silicon–carbon anode materials for lithium-ion batteries. R. Soc. open sci. **5** (2018) 172370.
27. Ma X, Liu M, Gan L, Tripathi PK, Zhao Y, Zhu D, Xu Z, Chen L, Novel mesoporous Si@C microspheres as anodes for lithium-ion batteries. Phys. Chem. Chem. Phys. **16** (2014) 4135–4142.
28. Seyed-Talebi SM, Kazeminezhad I, Beheshtian J, Theoretical prediction of silicene as a new candidate for the anode of lithium-ion batteries. Phys. Chem. Chem. Phys. **17** (2015) 29689–29696.
29. Shi L, Zhao TS, Xu A, Xu JB, Ab initio prediction of a silicene and graphene heterostructure as an anode material for Li- and Na-ion batteries. J. Mater. Chem. A, **4** (2016) 16377–16382.
30. Galashev AY, Ivanichkina KA, Silicene anodes for lithium-ion batteries on metal substrates. J. Electrochem. Soc. **167** (2020) 050510.
31. Galashev AY, Ivanichkina KA, Katin KP, Maslov MM, Computer test of a modified silicene/graphite anode for lithium-ion batteries. ACS Omega **5** (2020) 13207–13218.
32. Galashev AY, Ivanichkina KA, Computational investigation of a promising Si–Cu anode material. Phys. Chem. Chem. Phys. **21** (2019) 12310–12320.
33. Galashev AY, Ivanichkina KA, Computer study of atomic mechanisms of intercalation/deintercalation of Li ions in a silicene anode on an Ag (111) substrate. J. Electrochem. Soc. **165** (2018) A1788-A1796.
34. Galashev AY, Rakhmanova O.R. Promising two-dimensional nanocomposite for the anode of the lithium-ion batteries. Computer simulation. Physica E Low Dimens. Syst. Nanostruct. **126** (2021) 114446.
35. Grazianetti C, Cinquanta E, Molle A, Two-dimensional silicon: the advent of silicene. 2D Materials **3** (2016) 012001.
36. Xu S, Fan X, Liu J, Singh DJ, Jiang Q, Zheng W, Adsorption of Li on single-layer silicene for anodes of Li-ion batteries. Phys. Chem. Chem. Phys. **20** (2018) 8887–8896.
37. Galashev AY, Vorob'ev AS, First principle modeling of a silicene anode for lithium ion batteries. Electrochimica Acta **378** (2021) 138143 (1-10).
38. Tritsaris GA, Kaxiras E, Meng S, Wang E, Adsorption and diffusion of lithium on layered silicon for Li-ion storage. Nano Lett. **13** (2013) 2258–2263.
39. Zeng Z, Ma X, Chen J, Zeng Y, Yang D, Liu Y, Effects of heavy phosphorous-doping on mechanical properties of Czochralski silicon, J. Appl. Phys. **107** (2010) 123503.
40. Okamoto S, Ito A, Investigation of mechanical properties of nitrogen-containing graphene using molecular dynamics simulations. Proceeding of the International MultyConference of Engineers and Computer Scientists **1** (2012) IMECS, Hong Kong.
41. Liu B, Zhou K, Recent progress on graphene-analogous 2D nanomaterials: Properties, modeling and applications. Prog. Mater. Sci. **100** (2019) 99-169.
42. Gao J, Xu Z, Chen S, Bharathi MS, Zhang Y-W, Computational understanding of the growth of 2D materials. Adv. Theor. Simul. **1** (2018) 1800085.
43. Mannix AJ, Zhang Z, Guisinger NP, Yakobson B, Hersam MC, Borophene as a prototype for synthetic 2D materials development. Nat. Nanotechol. **13** (2018) 444–450.
44. Novoselov KS, Geim AK, Morozov SV, Jiang D, Zhang Y, Dubonos SV, Grigorieva IV, Firsov AA, Electric field effect in atomically thin carbon films. Science **306** (2004) 666–669.
45. Castro Neto AH, Guinea F, Peres NMR, Novoselov KS, Geim AK, The electronic properties of graphene. Rev. Mod. Phys. **81** (2009) 109–162.

46. Wallace PR, The band theory of graphite. Phys. Rev. **71** (1947) 622–634.
47. Bolotin KI, Sikes KJ, Jiang Z, Klima M, Fudenberg G, Hone J, Kim P, Stormer HL, Ultrahigh electron mobility in suspended graphene. Solid State Commun. **146** (2008) 351–355.
48. Weiss NO, Zhou H, Liao L, Jiang S, Huang Y, Duan X, Graphene: An emerging electronic material. Adv. Mater. **24** (2012) 5782–5825.
49. Novoselov KS, Geim AK, Morozov SV, Jiang D, Katsnelson MI, Grigorieva IV, Dubonos SV, Firsov AA, Two-dimensional gas of massless Dirac fermions in graphene. Nature **438** (2005) 197–200.
50. Zhang YB, Tan YW, Stormer HL, Kim P, Experimental observation of the quantum Hall effect and Berry's phase in graphene. Nature **438** (2005) 201–204.
51. Bolotin KI, Ghahari F, Shulman MD, Stomer HL, Kim P, Observation of the fractional quantum Hall effect in graphene. Nature **462** (2009) 196–199.
52. Du X, Skachko I, Duerr F, Luican A, Andrei EY, Fractional quantum Hall effect and insulating phase of Dirac electrons in graphene. Nature **462** (2009) 192–195.
53. Dean CR, Wang L, Maher P, Forsythe C, Ghahari F, et al. Hofstadter's butterfly and the fractal quantum Hall effectin moire superlattices. Nature, **497** (2013) 598–602.
54. Ponomarenko LA, Gorbachev RV, Yu GL, Elias DC, Jalil R, et al. Cloning of Dirac fermions in graphene superlattices. Nature **497** (2013) 594–597.
55. Hunt B, Sanchez-Yamagishi JD, Young AF, Yankowitz M, Leroy BJ et al. Massive Dirac fermions and Hofstadter butterfly in a van der Waals feterostructure. Science **340** (2013) 1427–1430.
56. Feldman BE, Levin AJ, Krauss B, Abanin D, Halperin BI, Smet JH, Yacoby A, Fractional quantum Hall phase transitions and four-flux states in graphene. Phys. Rev. Lett. **111** (2013) 076802.
57. Adam S, Hwang EH, Galitski VM, Das Sarma S, A self-consistent theory for graphene transport. P. Natl. Acad. Sci. USA **104** (2007) 18392–18397.
58. Dean CR, Young AF, Meric I, Lee C, Wang L, et al. Boron nitride substrates for high-quality graphene electronics. Nat. Nanotechnol. **5** (2010) 722–726.
59. Chen J-H, Jang C, Xiao SD, Ishigami M, Fuhrer MS, Intrinsic and extrinsic performance limits of graphene devices on SiO_2. Nat. Nanotechnol. **3** (2008) 206–209.
60. Morozov SV, Novoselov KS, Katsnelson MI, Schedin F, Elias DC, Jaszczak JA, Geim AK, Giant intrinsic carrier mobilities in graphene and its bilayer. Phys. Rev. Lett. **100** (2008) 016602.
61. Castro EV, Ochoa H, Katsnelson MI, Gorbachev RV, Elias DC, Novoselov KS, Geim AK, Guinea F, Limits on charge carrier mobility in suspended graphene due to flexural phonons. Phys. Rev. Lett. **105** (2010) 266601.
62. Li ZZ, Wang JY, Liu ZR, Intrinsic carrier mobility of Dirac cones: the limitations of deformation potential theory. J. Chem. Phys. **141** (2014) 144107.
63. Meyer JC, Geim AK, Katsnelson MI, Novoselov KS, Booth TJ, Roth S, The structure of suspended graphene sheets. Nature **446** (2007) 60–63.
64. Xu P, Neek-Amal M, Barber SD, Schoelz JK, Ackerman ML, et al. Unusual ultra-low-frequency fluctuations in freestanding graphene. Nat. Commun. **5** (2014) 3720.
65. Guinea F, Katsnelson MI, Vozmediano MAH, Midgap states and charge inhomogeneities in corrugated graphene. Phys. Rev. B **77** (2008) 075422.
66. Lui CH, Liu L, Mak KF, Flynn GW, Heinz TF, Ultraflat graphene. Nature **462** (2009) 339–341.
67. Zhang YB, Brar VW, Girit C, Zettl A, Crommie MF, Origin of spatial charge inhomogeneity in graphene. Nat. Phys. **5** (2009) 722–726.
68. Burson KM, Cullen WG, Adam S, Dean CR, Watanabe K, et al. Direct imaging of charged impurity density in common graphene substrates. Nano Lett. **13** (2013) 3576–3580.
69. Pereira VM, Neto AHC, Peres NMR, Tight-binding approach to uniaxial strain in graphene. Phys. Rev. B, **80** (2009) 045401.
70. Li Y, Jiang XW, Liu ZF, Liu Z, Strain effects in graphene and graphene nanoribbons: The underlying mechanism. Nano Res. **3** (2010) 545–556.
71. Pereira VM, Neto AHC, Strain engineering of graphene's electronic structure. Phys. Rev. Lett. **103** (2009) 046801.
72. Butler SZ, Hollen SM, Cao LY, Cui Y, Gupta JA et al. Progress, challenges, and opportunities in two-dimensional materials beyond graphene. Acs. Nano **7** (2013) 2898–2926.
73. Xu MS, Liang T, Shi MM, Chen H, Graphene-like two-dimensional materials. Chem. Rev. **113** (2013) 3766–3798.
74. Huang HQ, Duan WH, Liu ZR. The existence/absence of Dirac cones in graphynes. New J. Phys. **15** (2013) 023004.
75. Wang JY, Huang HQ, Duan WH, Liu Z, Identifying Dirac cones in carbon allotropes with square symmetry. J. Chem. Phys. **139** (2013) 184701.
76. Ma YD, Dai Y, Li XR, Sun Q, Huang B, Prediction of two-dimensional materials with half-metallic Dirac cones: $Ni_2C_8H_{12}$ and $Co_2C_8H_{12}$. Carbon, **73** (2014) 382–388.
77. Xu LC, Wang RZ, Miao MS, Wei X-L, Chen Y-P, et al. Two dimensional Dirac carbon allotropes from graphene. Nanoscale **6** (2014) 1113–1118.
78. Zhou XF, Dong X, Oganov AR, Zhu Q, Tian Y, et al. Semimetallic two-dimensional boron allotrope with massless Dirac fermions. Phys. Rev. Lett. **112** (2014) 085502.
79. Li WF, Guo M, Zhang G, Zhang YW, Gapless MoS_2 allotrope possessing both massless Dirac and heavy fermions. Phys. Rev. B, **89** (2014) 205402.
80. Wang ZF, Liu Z, Liu F, Organic topological insulators in organometallic lattices. Nat. Commun. **4** (2013) 1471.
81. Politano A, Chiarello G, Probing the Young's modulus and Poisson's ratio in graphene/metal interfaces and graphite: A comparative study. Nano Res. **8** (2015) 1847–1856.
82. Luo X, Schubert DW, Examining the contribution of factors affecting the electrical behavior of poly(methyl methacrylate)/graphene nanoplatelets composites. J. Appl. Polymer **138** (2021) 50694.

83. Qi W, Shapter JG, Wu Q, Yin T, Gao G, Cui D, Nanostructured anode materials for lithium-ion batteries: Principle, recent progress and future perspectives. J. Mater. Chem. A, **5** (2017) 19521–19540.
84. Lay GL, Padova PD, Resta A, Bruhn T, Vogt P, Epitaxial silicene: can it be strongly strained? J. Phys. D Appl. Phys. **45** (2012) 392001.
85. Peierls RE, Bemerkungen uber umwandlungs temperaturen, Helv. Phys. Acta **7** (1934) 81– 83.
86. Landau LD, Zur theorie der phase numwandlungen II, Phys. Z. Sowietunion **11** (1937) 26–35.
87. Yu M, Jayanthi CS, Wu SY, Bonding nature, structural optimization, and energetics studies of SiC graphitic-like layer structures and single/double walled nanotubes. arXiv:0901.3567 [cond-mat.mtrl-sci].
88. Feng B, Ding Z, Meng S, Yao Y, He X, Cheng P, et al. Evidence of silicene in honeycomb structures of silicon on Ag(111). Nano Lett. **12** (2012) 3507–3511.
89. Lalmi B, Oughaddou H, Enriquez H, Kara A, Vizzini Sb, Ealet Bn, et al. Epitaxial growth of a silicene sheet. Appl. Phys. Lett. **97** (2010) 223109.
90. Liu Z-L, Wang M-X, Liu C, Jia J-F, Vogt P, Quaresima C, et al. The fate of the $2\sqrt{3} \times 2\sqrt{3}$R(30°) silicene phase on Ag(111). APL Mater. **2** (2014) 092513.
91. Kawahara K, Shirasawa T, Arafune R, Lin CL, Takahashi T, Kawai M, et al. Determination of atomic positions in silicene on Ag(111) by low-energy electron diffraction. Surf. Sci. **623** (2014) 25–28.
92. Acun A, Poelsema B, Zandvliet HJW, van Gastel R. The instability of silicene on Ag(111). Appl. Phys. Lett. **103** (2013) 263119.
93. Zhao J, Liu H, Yu Z, Quhe R, Zhou S, Wang Y, et al. Rise of silicene: A competitive 2D material. Prog. Mater. Sci. **83** (2016) 24–151.
94. Kaltsas D, Tsetseris L, Dimoulas A, Structural evolution of single-layer films during deposition of silicon on silver: a first-principles study. J. Phys.: Condens. Matter. **24** (2012) 442001.
95. Liu Z-L, Wang M-X, Xu J-P, Ge J-F, Lay GL, Vogt P, et al. Various atomic structures of monolayer silicene fabricated on Ag(111). New J. Phys. **16** (2014) 075006.
96. Lin CL, Arafune R, Kawahara K, Tsukahara N, Minamitani E, Kim Y, et al. Structure of silicene grown on Ag(111). Appl. Phys. Exp. **5** (2012) 045802.
97. Chiappe D, Grazianetti C, Tallarida G, Fanciulli M, Molle A, Local electronic properties of corrugated silicene phases. Adv. Mater. **24** (2012) 5088–5093.
98. Resta A, Leoni T, Barth C, Ranguis A, Becker C, Bruhn T, et al. Atomic structures of silicene layers grown on Ag(111): scanning tunneling microscopy and noncontact atomic force microscopy observations. Sci. Rep. **3** (2013) 2399.
99. Zhuang J, Xu X, Du Y, Wu K, Chen L, Hao W, et al. Investigation of electron–phonon coupling in epitaxial silicene by in situ Raman spectroscopy. Phys. Rev. B **91** (2015)161409.
100. Grazianetti C, Chiappe D, Cinquanta E, Fanciulli M, Molle A, Nucleation and temperature-driven phase transitions of silicene superstructures on Ag(111). J. Phys.: Condens. Matter. **27** (2015) 255005.
101. Hvazdouski D, First-principles study of stability and electronic properties of single-element 2D materials. Doklady BGUIR, **19** (2022) 92–98.
102. Marianetti CA, Yevick HG, Failure mechanisms of graphene under tension. Phys. Rev. Lett. **105** (2010) 245502.
103. Jose D, Datta A, Understanding of the buckling distortions in silicene. J. Phys. Chem. C, **116** (2012) 24639–24648.
104. Botari T, Perim E, Autreto PAS, van Duin AC., Paupitz R, Galvao DS, Mechanical properties and fracture dynamics of silicene membranes. Phys. Chem. Chem. Phys. **16** (2014) 19417-19423.
105. Kohn W, Sham LJ, Self-consistent equations including exchange and correlation effects. Phys. Rev. **140** (1965) A1133–A1138.
106. Perdew J, K. Burke K, Ernzerhof M, Generalized gradient approximation made simple. Phys. Rev. Lett. **77** (1996) 3865–3868.
107. Jones RO, Gunnarsson O, The density functional formalism, its applications and prospects. Rev. Mod. Phys. **61** (1989) 689–746.
108. Nose SA, unified formulation of the constant temperature molecular dynamics methods. J. Chem. Phys. **81** (1984) 511–519.
109. Osborn TH, Farajian AA, Stability of lithiated silicene from first principles. J. Phys. Chem. C, **116** (2012) 22916–22920.
110. Kittel C. Introduction to Solid State Physics; Wiley: New York, 2005; p. 680.
111. Guerra C.F, Handgraaf JW, Baerends EJ, Bickelhaupt FM, Voronoi defor- mation density (VDD) charges: assessment of the Mulliken, Bader, Hirshfeld, Weinhold, and VDD methods for charge analysis. J. Comp. Chem. **25** (2003) 189–210.
112. Islam MS, Fisher CAJ, Lithium and sodium battery cathode materials: com- putational insights into voltage, diffusion and nanostructural properties. Chem. Soc. Rev. **43** (2014) 185–204.
113. Morris AJ, Grey CP, Pickard CJ, Thermodynamically stable lithium silicides and germanides from density-functional theory calculations. Phys. Rev. B, **90** (2014) 054111.
114. Guo YG, Hu JS, Wan LJ, Nanostructured Materials for Electrochemical Energy Conversion and Storage Devices. Adv. Mater. **20** (2008) 2878– 2887.
115. Ji L, Zhan L, Alcoutlabi M, Zhang X, Recent developments in nanostructured anode materials for rechargeable lithium-ion batteries. Energy Environ. Sci. **4** (2011) 2682–2699.
116. Xu W, Wang J, Ding F, Chen X, Nasybulin E, Zhang Y, Zhang JG, Lithium metal anodes for rechargeable batteries. Energy Environ. Sci. **7** (2014) 513–537.
117. Jing Y, Zhou Z, Cabrera CR, Chen Z, Graphene, inorganic graphene analogs and their composites for lithium ion batteries. J. Mater. Chem. A, **2** (2014) 12104–12122.

118. Jing Y, Zhou Z, Cabrera CR, Chen Z, Metallic VS_2 monolayer: A promising 2D anode material for lithium ion batteries. J. Phys. Chem. C, **117** (2013) 25409–25413.
119. Naguib M, Halim J, Lu J, Cook KM, Hultman L, Gogotsi Y, Barsoum MW, New two-dimensional niobium and vanadium carbides as promising materials for Li-ion batteries. J. Am. Chem. Soc., **135** (2013) 15966–15969.
120. Xie Y, Dall'Agnese Y, Naguib M, Gogotsi Y, Barsoum MW, Zhuang HL, Kent PR, Prediction and characterization of MXene nanosheet anodes for non-lithium-ion batteries. ACS Nano **8** (2014) 9606–9615.
121. Li W, Yang Y, Zhang G, Zhang YW, Ultrafast and directional diffusion of lithium in phosphorene for high-performance lithium-ion battery. Nano Lett. **15** (2015) 1691–1697.
122. Jiang HR, Lu Z, Wu MC, Ciucci F, Zhao TS, Borophene: A promising anode material offering high specific capacity and high rate capability for lithium-ion batteries. Nano Energy **23** (2016) 97–104.
123. Tang Q, Zhou Z, Shen P, Are MXenes promising anode materials for Li ion batteries? Computational studies on electronic properties and Li storage capability of Ti_3C_2 and $Ti_3C_2X_2$ (X = F, OH) monolayer. J. Am. Chem. Soc. **134** (2012) 16909–16916.
124. Slater MD, Kim D, Lee E, Johnson CS, Sodium-ion batteries. Adv. Funct. Mater. **23** (2013) 947–958.
125. Pan H, Hu YS, Chen L, Room-temperature stationary sodium-ion batteries for large-scale electric energy storage. Energy Environ. Sci. **6** (2013) 2338–2360.
126. Yabuuchi N, Kubota K, Dahbi M, Komaba S, Research development on sodium-ion batteries. Chem. Rev. **114** (2014) 11636–11682.
127. Yang E, Ji H, Jung Y, Two-dimensional transition metal dichalcogenide monolayers as promising sodium ion battery anodes. J. Phys. Chem. C, **119** (2015) 26374–26380.
128. Yang E, Ji H, Kim J, Kim H, Jung Y, Exploring the possibilities of two-dimensional transition metal carbides as anode materials for sodium batteries. Phys. Chem. Chem. Phys. **17** (2015) 5000–5005.
129. Yu YX, Prediction of mobility, enhanced storage capacity, and volume change during sodiation on interlayer-expanded functionalized Ti_3C_2 MXene anode materials for sodium-ion batteries. J. Phys. Chem. C, **120** (2016) 5288–5296.
130. Kulish VV, Malyi OI, Persson C, Wu P, Phosphorene as an anode material for Na-ion batteries: a first-principles study. Phys. Chem. Chem. Phys. **17** (2015) 13921–13928.
131. Shi L, Zhao TS, Xu A, Xu JB, Ab initio prediction of borophene as an extraordinary anode material exhibiting ultrafast directional sodium diffusion for sodium-based batteries. Science Bulletin, **61** (2016) 1138–1144.
132. Cahangirov S, Audiffred M, Tang P, Iacomino A, Duan W, Merino G, Rubio A, Electronic structure of silicene on Ag(111): Strong hybridization effects. Phys. Rev. B: Condens. Matter Mater. Phys. **88** (2013) 035432.
133. Cahangirov S, Topsakal M, Akt¨urk E, Sahin H, Ciraci S, Two- and one-dimensional honeycomb structures of silicon and germanium. Phys. Rev. Lett. **102** (2009) 236804.
134. Cai Y, Chuu CP, Wei CM, Chou MY, Stability and electronic properties of two-dimensional silicene and germanene on graphene. Phys. Rev. B: Condens. Matter Mater. Phys. **88** (2013) 245408.
135. Liu B, Baimova JA, Reddy CD, Law AWK, Dmitriev SV, Wu H, Zhou K, Interfacial thermal conductance of a silicene/graphene bilayer heterostructure and the effect of hydrogenation. ACS Appl. Mater. Interfaces, **6** (2014) 18180–18188.
136. Vogt P, De Padova P, Quaresima C, Avila J, Frantzeskakis E, Asensio MC, Resta A, Ealet B, Le Lay G, Silicene: Compelling experimental evidence for graphenelike two-dimensional silicon. Phys. Rev. Lett. **108** (2012) 155501.
137. Meng L, Wang Y, Zhang L, Du S, Wu R, Li L, Zhang Y, Buckled silicene formation on Ir(111). Nano Lett. **13** (2013) 685–690.
138. Nazzari D, Genser J, Ritter V, Bethge O, Bertagnolli E, Ramer G, Lendi B, Watanabe K, Taniguchi T, Rurali R, Kolibal M, Lugstein A, Highly biaxially strained silicene on Au(111). J. Phys. Chem. C **125** (2021) 9973–9980.
139. Huang L, Zhang Y, Zhang Y, Xu W, Que Y, Li E, Pan J, Wang Y, Liu Y, Du S, Pantelides ST, Gao H, Sequence of silicon monolayer structures grown on a Ru surface: from a herringbone structure to silicene. Nano Lett. **17** (2017) 116–1166.
140. Scalise E, Iordanidou K, Afanas VV, Stesmans A, Houssa M, Silicene on non-metallic substrates: Recent theoretical and experimental advances. Nano Res. **11** (2018) 1169–1182.
141. Fleurence A, Friedlein R, Ozaki T, Kawai H, Wang Y, Yamada-Takamura Y, Experimental evidence for epitaxial silicene on diboride thin films. Phys. Rev. Lett. **108** (2012) 245501.
142. Aizawa T, Suehara S, Otani S, Silicene on zirconium carbide (111), J. Phys. Chem. C. **118** (2014) 23049–23057.
143. De Crescenzi M, Berbezier I, Scarselli M, Castrucci P, Abbarchi M, Ronda A, Jardali F, Park J, Vach H, Fisica D, Tor R, Formation of silicene nanosheets on graphite, ACS Nano **10** (2016) 11163–11171.
144. Galashev AE, Ivanichkina KA, Computer study of silicene applicability in electrochemical devices. J. Struct. Chem. **61** (2020) 659–667.
145. Galashev AY, Zaikov YuP, New Si–Cu and Si–Ni anode materials for lithium-ion batteries. J. Appl. Electrochem. **49** (2019) 1027–1034.
146. Galashev AY, Ivanichkina KA, Computer test of a new silicene anode for lithium-ion batteries. ChemElectroChem **6** (2019) 1525-1535.
147. Galashev AE, Rakhmanjva OR, Stability of a two-layer silicene on a nickel substrate upon intercalation of lithium. Glass Phys. Chem. **46** (2020) 321–328.
148. Galashev AY, Ivanichkina KA, Vorob'ev AS, Rakhmanjva OR, Katin KP, Maslov MM, Improved lithium-ion batteries and their communication with hydrogen power. Int. J. Hydrogen Energy **46** (2021) 17019–17036.

149. Galashev AY, Rakhmanjva OR, Ivanichkina KA, Graphene and graphite supports for silicene stabilization: A computation study. J. Struct. Chem. **59** (2018) 877–883.
150. Galashev AY, Ivanichkina KA, Numerical simulation of the structure and mechanical properties of silicene layers on graphite during the lithium ion motion. Phys. Solid State **61** (2019) 233–243.
151. Galashev AY, Suzdaltsev AV, Ivanichkina KA, Design of the high performance microbattery with silicene anode. Mater. Sci. & Eng. B **261** (2020) 114718.
152. Galashev AY, Ivanichkina KA, Katin KP, Maslov MM, Computational study of lithium intercalation in silicene channels on a carbon substrate after nuclear transmutation doping. Computation **7** (2019) 60.
153. Galashev AY, Numerical simulation of a 2D layered anode for use in lithium-ion batteries. Int.J. Comput. Meth. **18** (2021), 2150032.
154. Galashev AE, Rakhmanjva OR, Katin KP, Maslov MM, Zaikov YuP, Effect of an electric field on a lithium ion in a channel of the doped silicene–graphite system. Rus. J. Phys. Chem. B **14** (2020) 1055–1062.
155. Galashev AY, Rakhmanjva OR, Two-layer silicene on the SiC substrate: lithiation investigation in the molecular dynamics experiment. ChemPhysChem **26** (2022) e202200250. https://doi.org/10.1002/cphc.202200250
156. Thuy Tran NT, Gumbs G, Nguyen DK, Lin M-F, Fundamental properties of metal-adsorbed silicene: A DFT study, ACS Omega **5** (2020) 13760–13769.
157. Lin H, Qiu W, Liu J, Yu L, Gao S, Yao H, Chen Y, Silicene: Wet-chemical exfoliation synthesis and biodegradable tumor nanomedicine. Adv. Mater. **31** (2019) 1903013.
158. Galashev AY, Vorob'ev AS, DFT study of silicene on metal (Al, Ag, Au) substrates of various thicknesses. Phys. Lett. A **408** (2021) 127487.
159. Galashev A, Vorob'ev A, An Ab initio study of lithization of two-dimensional silicon–carbon anode material for lithium-ion batteries. Materials **14** (2021) 6649.
160. Galashev A, Vorob'ev A, Electronic properties and structure of silicene on Cu and Ni substrates. Materials **15** (2022) 3863.
161. Soler JM, Artacho E, Gale JD, Garcia A, Junquera J, Ordejon P, Sanchez-Portal D, The SIESTA method for ab initio order-N materials simulation, J. Phys. Condens. Matter **14** (2002) 2745–2779.
162. Kresse G, Furthmüller J, Efficient iterative schemes for *ab initio* total-energy calculations using a plane-wave basis set. Phys. Rev. B **54** (1996) 11169–11186.
163. Lubarda VA, On the effective lattice parameter of binary alloys. Mech. Mater. **35** (2003) 53–68.
164. Flynn S., Lennon A. Copper penetration in laser-doped selective-emitter silicon solar cells with plated nickel barrier layers. Solar Energy Materials & Solar Cells **130** (2014) 309–316.
165. Cheng YR, Chen WJ, Ohdaira K, Higashimine K, Barrier properties of electroplating nickel layer for copper metallization in silicon solar cells. Int. J. Electrochem. Sci. **13** (2018) 11516–11525.
166. Kuchuk AV, Borowicz P, Wzorek M, Borysiewicz M, Ratajczak R, Golaszewska K, et al. Ni-based ohmic contacts to *n*-type 4H-SiC: The formation mechanism and thermal stability. Adv. Cond. Mat. Phys. **2016** (2016) 1-26.
167. Galashev AY, Vorob'ev AS, An *ab initio* study of the interaction of graphene and silicene with one-, two-, and three-layer planar silicon carbide. Physica E: Low-dimens. Syst. Nanostruct. **138** (2022) 115120.
168. Zaminpayma E, Nayebi P, Band gap engineering in silicene: A theoretical study of densityfunctional tight-binding theory. Phys. E: Low-dimens. Syst. Nanostruct. **84** (2016) 555–563.
169. Galashev AY, Vorob'ev AS, Electronic and mechanical properties of silicene after nuclear transmutation doping with phosphorus. J. Mater. Sci. **55** (2020) 11367–11381.
170. Lin C-L, Arafune R, Kawahara K, Tsukahara N, Minamitani E, Kim Y, Takagi N, Kawai M, Structure of silicene grown on Ag(111). Appl. Phys. Express **5** (2012) 045802.
171. Jamgotchian H, Colignon Y, Hamzaoui N, Ealet B, Hoarau JY, Aufray B, Bib´erian JP, Growth of silicene layers on Ag(111): unexpected effect of the substrate temperature J. Phys. Condens. Matter. **24** (2012) 172001.
172. Le Lay G, De Padova P, Resta A, Bruhn T, Vogt P, Epitaxial silicene: can it be strongly strained? J. Phys. D Appl. Phys. **45** (2012) 392001.
173. Okamoto H, Massalski TB, The Au–Si (Gold-Silicon) system. Bull. Alloy Phase Diagram **4** (1983) 190–198.
174. Becke AD, Edgecombe KE, A simple measure of electron localization in atomic and molecular systems. J. Chem. Phys. **92** (1990) 5397–5403.
175. Stephan R, Hanf M-C, Sonnet P, Spatial analysis of interactions at the silicene/Ag interface: first principles study. J. Phys.: Condens. Matter. **27** (2015) 015002.
176. Lin CL, Arafune R, Kawahara K, Kanno M, Tsukahara N, Minamitani E, Kim Y, Kawai M, Takagi N, Substrate-induced symmetry breaking in silicene. Phys.Rev. Lett. **110** (2013) 076801.
177. Johnson NW, Vogt P, Resta A, De Padova P, Perez I, Muir D, Kurmaev EZ, Le Lay G, Moewes A, The metallic nature of epitaxial silicene monolayers on Ag (111). Adv. Funct.Mater. **24** (2014) 5253–5259.
178. Majzik Z, Tchalala MR, Svec M, Hapala P, Enriquez H, Kara A, Mayne AJ, Dujardin G, Jelinek P, Oughaddou H, Combined AFM and STM measurements of a silicene sheet grown on the Ag (111) surface. J. Phys.: Condens. Matter. **25** (2013) 225301.
179. Hu W, Xia N, Wu X, Li Z, Yang J, Silicene as a highly sensitive molecule sensor for NH_3, NO and NO_2. Phys. Chem. Chem. Phys. **16** (2014) 6957–6962.
180. Osborn TH, Farajian AA, Silicene nanoribbons as carbon monoxide nanosensors with molecular resolution. Nano Res. **7** (2014) 945–952.
181. Feng JW, Liu Y-J, Wang H-X, Zhao J-X, Cai Q-H, Wang X-Z, Gas adsorption on silicene: A theoretical study. Comput. Mater. Sci. **87** (2014) 218–226.
182. Oughaddou H, Enriquez H, Tchalalaa MR, Yildirim H, Mayne AJ, Bendounan A, Dujardin G, Ait Ali M, Kara.A,

Silicene, a promising new 2D material. Prog. Surf. Sci. **90** (2015) 46–83.
183. Ezawa M, Valley-polarized metals and quantum anomalous Hall effect in silicene. Phys. Rev. Lett. **109** (2012) 055502.
184. Pan L. Liu HJ, Tan XJ, Lv HY, Shi J, Tang XF, Zheng G, Thermoelectric properties of armchair and zigzag silicene nanoribbons. Phys. Chem. Chem. Phys. **14** (2012) 13588–13593.
185. Tao L, Cinquanta E, Chiappe D, Grazianetti C, Fanciulli M, Dubey M, Molle A, Akinwande D, Silicene field-effect transistors operating at room temperature. Nat. Nanotechnol. **10** (2015) 227–231.
186. Bai J, Tanaka H, Zeng XC, Graphene-like bilayer hexagonal silicon polymorph. Nano Res. **3** (2010) 694–700.
187. Fu H, Zhang J, Ding Z, Li H, S Meng S, Stacking-dependent electronic structure of bilayer silicene. Appl. Phys. Lett. **104** (2014) 131904.
188. Luo W, Ma Y, Gong X, Xiang H, Prediction of silicon-based layered structures for optoelectronic applications. J. Am. Chem. Soc. **136** (2014) 15992–15997.
189. Sakai Y, Oshiyama A, Structural stability and energy-gap modulation through atomic protrusion in freestanding bilayer silicene. Phys. Rev. B **91** (2015) 201405.
190. Pandey KC, New π-bonded chain model for Si(111)-(2×1) surface. Phys. Rev. Lett. **47** (1981) 1913–1917.
191. Stich I, Payne MC, King-Smith RD, Lin J-S, Clarke LJ, *Ab initio* total-energy calculations for extremely large systems: Application to the Takayanagi reconstruction of Si(111). Phys. Rev. Lett. **68** (1992) 1351–1354.
192. Brommer KD, Needels M, Larson BE, Joannopoulos JD, *Ab initio* theory of the Si(111)-(7×7) surface reconstruction: A challenge for massively parallel computation. Phys. Rev. Lett. **68** (1992) 1355–1358.
193. Takayanagi K, Tanishiro Y, Takahashi M, Takahashi S, Structural analysis of Si(111)-7×7 by UHV-transmission electron diffraction and microscopy. J. Vac. Sci. Technol. **4** (1985) 1502.
194. Takayanagi K, Tanishiro Y, Takahashi S, Takahashi M, Structure analysis of Si(111)-7 × 7 reconstructed surface by transmission electron diffraction. Surf. Sci. **164** (1985) 367–392.
195. Hybertsen MS, Louie SG, First-principles theory of quasiparticles: Calculation of band gaps in semiconductors and insulators. Phys. Rev. Lett. **55** (1985) 1418–1421.
196. De Padova P, Generosi A, Paci B, Ottaviani C, Quaresima C, Olivieri B, Salomon E, Angot T, Le Lay G, Multilayer silicene: clear evidence. 2D Materials **3** (2016) 031011.
197. Zheng F-B, Zhang C-W, The electronic and magnetic properties of functionalized silicene: a first-principles study. Nanoscale Res. Lett. **7** (2012) 422.
198. Zhu J, Schwingenschlög U, Silicene for Na-ion battery applications. 2D Materials **3** (2016) 035012.
199. Ding Y, Wang Y, Unusual structural and electronic properties of porous silicene and germanene: insights from first-principles calculations. Nanoscale Res. Lett. **10** (2015) 13.
200. Agubra V, Fergus J, Lithium ion battery anode aging mechanisms. Materials **6** (2013) 1310–1325.
201. An SJ, Li J, Daniel C, Mohanty D, Nagpure S, Wood DL, The state of understanding of the lithium-ion-battery graphite solid electrolyte interphase (SEI) and its relationship to formation cycling. Carbon **105** (2016) 52–76.
202. Shi Q, Liu W, Qu Q, Gao T, Wang Y, Liu G, Battaglia VS, Zheng H, Robust solid/electrolyte interphase on graphite anode to suppress lithium inventory loss in lithium-ion batteries. Carbon **111** (2017) 291–298.
203. Chang H, Wu Y-R, Han X, Yi T-F, Recent developments in advanced anode materials for lithium-ion batteries. Energy Mater. **1** (2021) 100003.
204. Kummer M, Badillo JP, Schmitz A, et al. Silicon/polyaniline nanocomposites as anode material for lithium ion batteries. J. Electrochem. Soc. **161** (2013) A40-A45.
205. Zhou L, Zhang K, Hu Z, et al. Recent Developments on and prospects for electrode materials with hierarchical structures for lithiumion batteries. Adv. Energy Mater. **8** (2018) 1701415.
206. Kim H, Lee E, Sun Y, Recent advances in the Si-based nanocomposite materials as high capacity anode materials for lithium ion batteries. Mater. Today **17** (2014) 285–297.
207. Su X, Wu Q, Li J, et al. Silicon-based nanomaterials for lithium-ion batteries: a review. Adv. Energy Mater. **4** (2014) 1300882.
208. Terranova ML, Orlanducci S, Tamburri E, Guglielmotti V, Rossi M, Si/C hybrid nanostructures for Li-ion anodes: an overview. J. Power Sources **246** (2014) 167-177.
209. Peng Q, Wen X-D, De S, Mechanical stabilities of silicene. RSC Adv. **3** (2013) 13772-13781.
210. Yoo S.H, Lee B, Kang K, Density functional theory study of the mechanical behavior of silicene and development of a Tersoff interatomic potential model tailored for elastic behavior. Nanotechnology **32** (2021) 295702.
211. Wortman JJ, Evans RA, Young's modulus, shear modulus, and Poisson's ratio in silicon and germanium. J. Appl. Phys. **36** (1965) 153–156.
212. Zhang X, Xie H, Hu M, Bao H, Yue S et al. Thermal conductivity of silicene calculated using an optimized Stillinger-Weber potential. Phys. Rev. B **89(5)** (2014) 054310.
213. Anufriev R, Wu Y, Ordonez-Miranda J, Nomura M, Nanoscale limit of the thermal conductivity in crystalline silicon carbide membranes, nanowires, and phononic crystals. NPG Asia Mater. **14** (2022) 35.
214. Jannatul Islam ASM, Sherajul Islam Md, Ferdous N, Park J, Hashimoto A, Vacancy-induced thermal transport in two-dimensional silicon carbide: a reverse non-equilibrium molecular dynamics study. Phys. Chem. Chem. Phys. **22** (2020) 13592–13602.
215. Pender JP, Jha G, Youn DH, Ziegler JM, Andoni I, Choi EJ, Heller A, Dunn BS, Weiss PS, Penner RM, Mullins CB, Electrode degradation in lithium-ion batteries. ACS Nano **14** (2020) 1243–1295.

216. Ertural C, Stoffel RP, Muller PC, Vogt CA, Dronskowski R First-principles plane-wave-based exploration of cathode and anode materials for Li and Na-ion batteries involving complex nitrogen-based anions. Chem. Mater. **34(2)** (2022) 652–668.
217. Budnyak TM, Slabon A, Sipponen MH, Lignin-inorganic interfaces: Chemistry and applications from adsorbents to catalysts and energy storage materials. ChemSusChem **13(17)** (2020) 4344–4355.
218. Lin D, Liu Y, Cui Y, Reviving the lithium metal anode for high-energy batteries. Nature Nanotechnol. **12(3)** (2017) 194–206.
219. Lenchuk O, Adelhelm P, Mollenhauer D, New insights into the origin of unstable sodium graphite intercalation compounds. Phys. Chem. Chem. Phys. **21(35)** (2019) 19378–19390.
220. Li Y, Lu Y, Adelhelm P, Titirici M-M, Hu Y-S, Intercalation chemistry of graphite: Alkali metal ions and beyond. Chem. Soc. Rev. **48(17)** (2019) 4655–4687.
221. Kubota K, Dahbi M, Hosaka T, Kumakura S, Komaba S, Towards K-ion and Na-ion batteries as "Beyond Li-ion". Chem. Rec. **18(4)** (2018) 459–479.
222. Wang Z, Selbach SM, Grande T, Van der Waals density functional study of the energetics of alkali metal intercalation in graphite. RSC Adv. **4(8)** (2014) 4069–4079.
223. Kim H, Yoon G, Lim K, Kang K, A comparative study of graphite electrodes using the co-intercalation phenomenon for rechargeable Li, Na and K batteries. Chem. Commun. **52(85)** (2016) 12618–12621.